Supplementary information.

Molecular asymmetry and rigidification as strategies to activate and enhance thermally activated delayed fluorescence in deep-blue MR-TADF emitters

Rangani Wathsala Weerasinghe,[a] John Marques Dos Santos,[b] Youhei Chitose, [a,c] Tomas Matulaitis,[b] Stuart L. Warriner,[f] Debasish Barman,[a] Chin-Yiu Chan,[d,e]* Youichi Tsuchiya,[a]* Eli Zysman-Colman[b]* and Chihaya Adachi[a]*

[a] Center for Organic Photonics and Electronics Research (OPERA), Kyushu University, Motooka, Nishi, Fukuoka 819-0395, Japan

[b] Organic Semiconductor Centre, EaStCHEM School of Chemistry, University of St Andrews, St Andrews, KY16 9ST, UK, Email: eli.zysman-colman@st-andrews.ac.uk

[c] Department of Applied Chemistry, Graduate School of Engineering, Center for Molecular Systems (CMS), Kyushu University, 744 Motooka, Nishi, Fukuoka 819-0395, Japan

[d] Department of Chemistry, City University of Hong Kong, Tat Chee Avenue, Kowloon, Hong Kong, China

[e] Department of Chemistry, City University of Hong Kong, Tat Chee Avenue, Kowloon, Hong Kong, China

[f] School of Chemistry, University of Leeds, Leeds, LS2 9JT, UK.

Contents

1. Experimental Section

Theoretical calculations. Calculations were firstly performed using Density Functional Theory (DFT) within Gaussian 16 revision A. 03[1] and then with the second order algebraic diagrammatic construction Spin-Component Scaling (ADC(2)-SCS)[2] method using the Turbomole/7.5 package.[3] For the DFT calculations, the ground state and excited singlet state were optimized using the PBE0[4] functional and the 6-31G(d,p) basis set,[5] and the excited-state calculations were performed using Time-Dependent DFT within the Tamm-Dancoff approximation (TDADFT)[6,7] with the same functional and basis set as for the ground-state geometry optimization in the gas phase. The molecular orbital distributions were visualized with Gaussview 5.0.[8] For the ADC(2) calculations, the ground states was optimized using the ADC(2)-SCS functional and the cc-pVDZ basis set in the gas phase based on the geometry calculated by DFT.[2] Vertical transitions to the excited states were performed based on the ground-state optimized structure. Difference density plots were used to visualize change in electronic density between the ground and excited state and were visualized using the VESTA package.[9] The calculations were submitted and processed using the Silico v4 software package,[10] which incorporates a number of publicly available software libraries, including: cclib[11] for parsing of result files, VMD[12] and Tachyon[13] for 3D rendering, Matplotlib[14] for the plotting of graphs, Open Babel[15] and Pybel[16] for file interconversion. For spin-orbit coupling (SOC) matrix elements between singlet and triplet excited states, S_0, S_1, T_1 and T_2 geometry optimizations were performed at the PBE0/6-31G(d,p) level of theory [4,5] in the gas phase, using Gaussian 16 revision A. 03.[1] TDA-DFT[6,7] calculations at the PBE0/6-31G(d,p) level[4,5] and SCS-CC2 [17] calculations with cc-pVDZ[5] basis set were used for SOC matrix element calculation using ORCA 5.0.3 program.[18]

General synthetic procedures. All reagents and solvents were obtained from commercial sources and used as received. Air-sensitive reactions were performed under a nitrogen atmosphere using Schlenk techniques, no special precautions were taken to exclude air or moisture during work-up. DCM was obtained from a MBraun SPS5 solvent purification system. Flash column chromatography was carried out using silica gel (Silia-P from Silicycle, 60 Å, 40-63 μm). Analytical thin-layer-chromatography (TLC) was performed with silica plates with aluminum backings (250 μm with F-254 indicator). TLC visualization was accomplished by 254/365 nm UV lamp. HPLC analysis was conducted on a Shimadzu LC-40 HPLC equipped with a Shim-pack GIST 3μm C18 reverse phase analytical column. GCMS analysis was conducted using a Shimadzu QP2010SE GC-MS equipped with a Shimadzu SH-Rtx-1 column (30 m × 0.25 mm). ^{1}H and ^{13}C NMR spectra were recorded on a Bruker Advance spectrometer (400 MHz for ^{1}H and either 101 or 126 MHz for ^{13}C). The following abbreviations have been used for multiplicity assignments: "s" for singlet, "d" for doublet, "t" for triplet, "m" for multiplet, and "dd" for doublet of doublets. ^{1}H and ^{13}C NMR spectra

were referenced residual solvent peaks with respect to TMS (δ = 0 ppm). Melting points were measured using open-ended capillaries on an Electrothermal 1101D Mel-Temp apparatus and are uncorrected. High-resolution mass spectrometry (HRMS) was performed in the School of Chemistry of the University of Leeds. HPLC analysis was conducted on a Shimadzu LC-40 HPLC equipped with a GPC using a Shim-pack GPC-803 column with THF as mobile phase.

Electrochemistry Measurements. Cyclic Voltammetry (CV) analysis was performed on an Electrochemical Analyzer potentiostat model 620E from CH Instruments at a sweep rate of 100 mV s^{-1}. Differential pulse voltammetry (DPV) was conducted with an increment potential of 0.01 V and a pulse amplitude, width, and period of 50 mV, 0.06, and 0.5 s, respectively. Samples were prepared as dichloromethane solutions, degassed by sparging with dichloromethane N_2 for 5 minutes before measurements. All measurements were performed using 0.1 M dichloromethane solution of tetrabutylammonium hexafluorophosphate ([^{n}Bu$_4$N]PF$_6$). An Ag/Ag$^+$ electrode was used as the reference electrode, while a glassy carbon electrode and a platinum wire were used as the working electrode and counter electrode, respectively. The redox potentials are reported relative to a saturated calomel electrode (SCE) with a ferrocenium/ferrocene (Fc/Fc$^+$) redox couple as the internal standard (0.46 V vs. SCE).[19] The HOMO and LUMO energies were determined using the relation $E_{\text{HOMO/LUMO}} = -(E_{\text{ox}} / E_{\text{red}} + 4.8)$ eV, where E_{ox} and E_{red} are the onset of anodic and cathodic peak potentials, respectively calculated from DPV relative to Fc/Fc$^+$.[20]
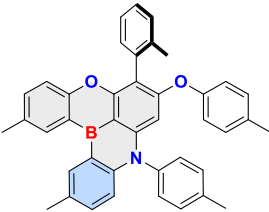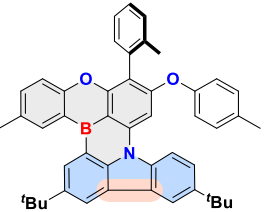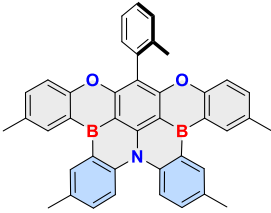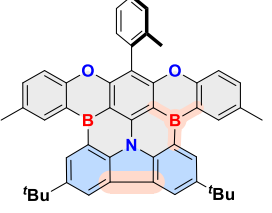
Photophysical measurements. Optically dilute solutions of concentrations on the order of 10^{-5} were prepared in spectroscopic or HPLC grade solvents for absorption and emission analysis. Organic thin films for photophysical measurements (except for streak camera measurements) were fabricated on quartz substrates, which were pre-cleaned using acetone and isopropanol followed by 15 min UV treatment (NL-UV253, Nippon Laser & Electronics Lab., Japan) just prior to the film preparation to remove adsorbed organic species before deposition. Thin films for the streak camera measurements were prepared on silicon substrates. All the films were fabricated by vacuum thermal evaporation at a pressure below 10^{-4} Pa. UV-vis absorption spectra were recorded at room temperature using a Lambda 950-PKA spectrophotometer (Perkin-Elmer, USA). 1 cm quartz cuvettes were used for the solutions. Stead-state emission spectra were recorded using an FP-8600 fluorometer (JASCO, Japan). Phosphorescence measurements were taken at 77 K (delay 115 ms, gate 150 ms). A Quantaurus-QY C11347-01 (Hamamatsu Photonics, Japan) integrating sphere was used to measure the absolute PL quantum yields. The transient photoluminescence decay characteristics were measured with a Quantaurus-Tau C11367-03 (Hamamatsu Photonics, Japan) instrument and a streak camera system (C10910-01, Hamamatsu Photonics, Hamamatsu, Japan) with a third harmonic YAG laser (355 nm, 10 Hz, PL-2250, EKSPLA, Lithuania) as an excitation source. The thicknesses of all the films were measured using Variable-angle spectroscopic ellipsometry with an M-

2000U (J.A. Woollam Co. Inc., USA) instrument. The angular dependent PL properties were simulated using SETFOS 5.1 (Fluxim) software to determine the dipole orientation of the doped films and consequently to determine the light outcoupling efficiency. (EQE = $\gamma \times \eta_v \times \Phi_{PL} \times \eta_{OC}$, where γ is the charge balance and η_γ denotes the efficiency of radiative exciton production).

Device fabrication and measurement of electroluminescence characteristics. OLEDs were fabricated on glass substrates coated with a patterned transparent ITO conductive layer (50 nm). ITO glass substrates were cleaned using detergent, followed by de-ionized water, acetone, and isopropanol and dried with isopropanol. Then, they were subjected to the UV treatment for 15 min just prior to the device fabrication. The devices were fabricated by using vacuum deposition under 1.0×10^{-5} Pa. The current density-voltage-luminance (*J-V-L*) characteristics of the OLEDs were assessed using a source meter (Keysight B2911A, Keysight Technologies, USA) and a luminance meter (CS-2000, Konica Minolta, Japan) at a constant DC current at room temperature.

2. Synthesis and Characterization

Table **S1.** Molecular structures of **1B-DTACrs**, **2B-DTACrs**, **1B-CzCrs**, and **2B-CzCrs**.

	Diphenylamine-containing compounds[21] (Previous study)	Carbazole-containing compounds (This study)
Asymmetric	 **1B-DTACrs**	 **1B-CzCrs**
Symmetric	 **2B-DTACrs**	 **2B-CzCrs**

The synthetic route to **1B-CzCrs** and **2B-CzCrs** is outlined in Figure **S1.** 4,4'-((5-Bromo-1,3-phenylene) bis(oxy))bis(methylbenzene) (compound **1**), of which the synthesis was reported in our previous study[21] was first reacted with 3,6-di-*tert*-butylcarbazole (compound **2**) by palladium-catalyzed Buchwald-Hartwig cross-coupling reaction. Then, bromination of compound **3** was performed using N-bromosuccinimide at low temperatures. The brominated compound **4** was further coupled with *o*-tolylboronic acid, resulting in compound **5** in a good yield (95%). **1B-CzCrs** and **2B-CzCrs** were obtained following a bora-Friedel-Crafts reaction with the help of BI$_3$, in 15 and 12% yield, respectively.
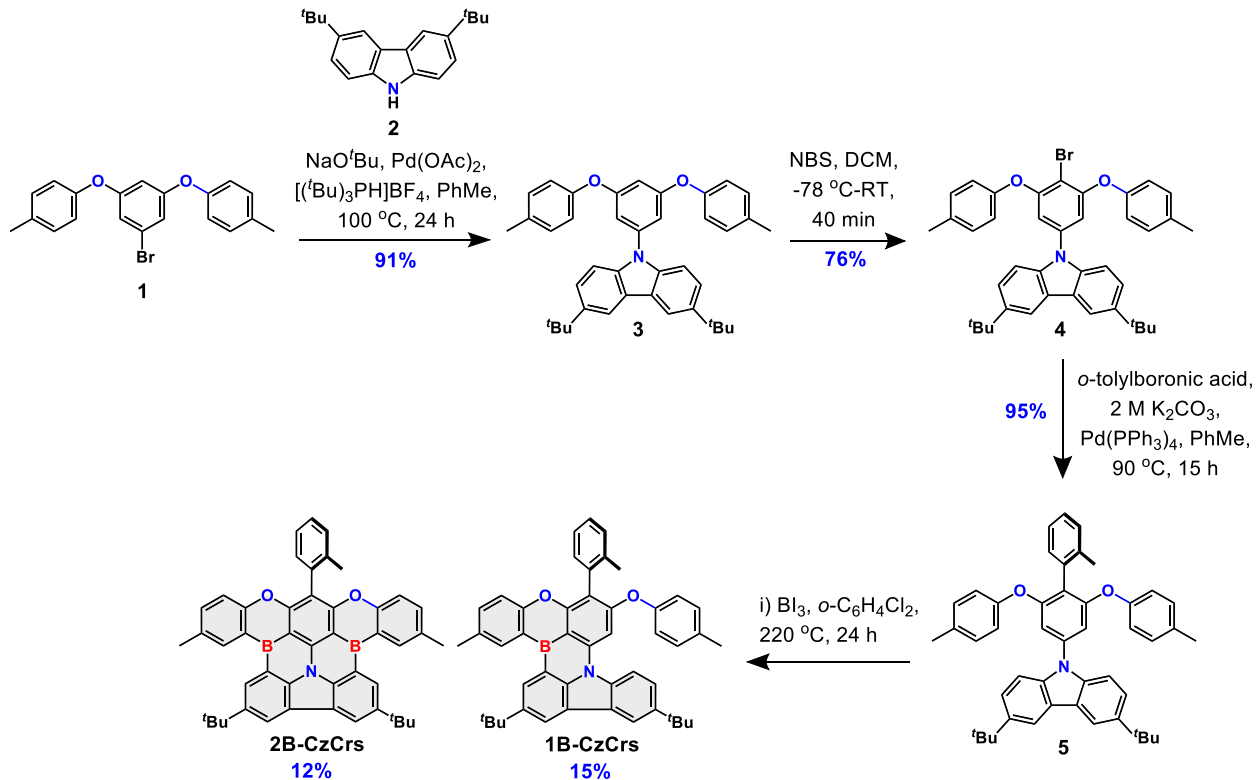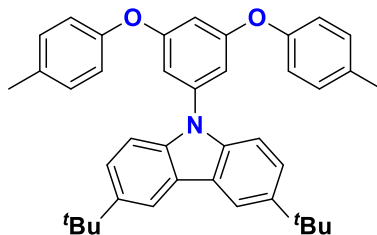

Figure **S1**. The synthetic route of the **1B-CzCrs** and **2B-CzCrs**.

9-(3,5-bis(p-tolyloxy)phenyl)-3,6-di-*tert*-butyl-9H-carbazole (3)

To a Schlenk flask under nitrogen was added, 4,4'-((5-bromo-1,3-phenylene)bis(oxy))bis(methylbenzene) (**1**) (12.35 g, 33.45 mmol, 1 equiv.), 3,6-di-*tert*-butyl-9H-carbazole (11.21 g, 40.13 mmol, 1.2 equiv.), Sodium *tert*-butoxide (9.64 g, 100.3 mmol, 3.00 equiv.), Pd(OAc)$_2$ (0.660 g, 2.943 mmol, 0.088 equiv.), [(^{t}Bu)$_3$PH]BF$_4$ (0.349 g, 1.204 mmol, 0.036 equiv.) and 100 mL toluene. After stirring at 110 °C for 24 h, the reaction mixture was brought to RT and extracted with 200 mL DCM. This was then washed 3 times with 150 mL DI water and the organic layer was dried over sodium sulfate. The crude mixture was purified by silica gel flash column chromatography using DCM:hexane = 2:8. The corresponding fractions were combined and concentrated under reduced pressure to afford a white solid (17.3 g), which was filtered and dried. **Yield**: 91%. **R$_f$:** 0.39 (DCM:hexane = 20:80 on silica gel). **Mp**: 176-179 °C. **^{1}H NMR (400 MHz, CDCl$_3$)** δ 8.12 (dd, J = 2.0, 0.6 Hz, 2H), 7.48 (dd, J = 8.7, 1.9 Hz, 2H), 7.41 (dd, J = 8.7, 0.7 Hz, 2H), 7.21 – 7.14 (m, 4H), 7.07 – 7.01 (m, 4H), 6.88 (d, J = 2.2 Hz, 2H), 6.72 (t, J = 2.2 Hz, 1H), 2.34 (s, 6H), 1.48 (s, 18H). **^{13}C NMR (101 MHz, CDCl$_3$) δ** ^{13}C NMR (101 MHz, Chloroform-*d*) δ 160, 153, 143, 140, 138, 133, 130, 123, 123, 119, 116, 110, 109, 106, 34, 32, 20. **HR-MS [M]$^+$ Calculated:** (C$_{40}$H$_{42}$NO$_2$) 568.3216; **Found:** 568.3201.

9-(4-bromo-3,5-bis(p-tolyloxy)phenyl)-3,6-di-*tert*-butyl-9H-carbazole (4)
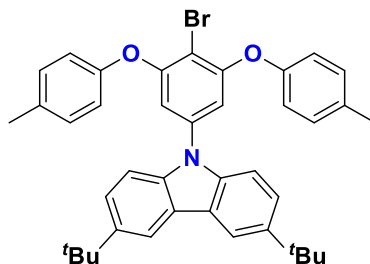
Compound **3** (5.00 g, 8.80 mmol, 1 equiv.) was added to 50 mL DCM in an RB flask in air and cooled to -78 °C. To this solution, *N*-bromosuccinimide (1.72 g, 9.69 mmol, 1.1 equiv.) was added and stirred at that temperature for 10 min, followed by stirring at RT for 30 min. The completion of the reaction was confirmed by thin layer chromatography. The reaction was quenched by the addition of 50 mL DCM and 100 mL 5%

NaOH solution. The organic layer was then separated and washed with DI water (100 mL × 2). The DCM layer was then concentrated under reduced pressure followed by sonication in 50 mL methanol for 10 min. The resultant white solid was filtered and washed with methanol (30 mL) to give 4.5 g of compound **4**. **Yield**: 79%. **R$_f$**: 0.54 (DCM:hexane = 20:80 on silica gel). **Mp**: 185-188 °C. **^{1}H NMR (400 MHz, CDCl$_3$)** δ 8.06 (dd, J = 1.9, 0.8 Hz, 2H), 7.44 – 7.39 (m, 2H), 7.25 – 7.21 (m, 2H), 7.20 – 7.14 (m, 4H), 7.07 – 7.00 (m, 4H), 6.81 (d, J = 0.8 Hz, 2H), 2.32 (s, 6H), 1.44 (s, 18H). **^{13}C NMR (101 MHz, CDCl$_3$)** δ 157, 143, 138, 138, 134, 130, 123, 123, 119, 116, 111, 109, 103, 34, 31, 20. **HR-MS [M]$^+$ Calculated:** (C$_{40}$H$_{41}$BrNO$_2$) 646.2315; **Found:** 646.2313.

3,6-di-*tert*-butyl-9-(2'-methyl-2,6-bis(p-tolyloxy)-[1,1'-biphenyl]-4-yl)-9H-carbazole (5)
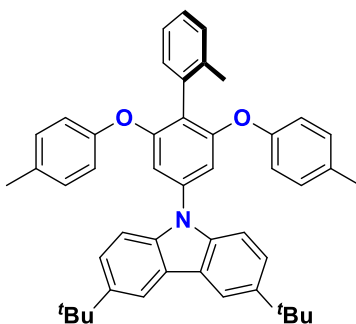
Compound **4** (8.00 g, 12.37 mmol, 1.00 equiv.), *o*-tolylboronic acid (4.04 g, 18.5 mmol, 1.5 equiv.), K$_2$CO$_3$ (5.13 g, 37.1 mmol, 3.0 equiv.) were added to a nitrogen degassed mixture of toluene and water (50 mL:10 mL) in an RB flask. To this solution under the protection of nitrogen, Pd(PPh$_3$)$_4$ (0.714 g, 0.618 mmol, 0.05 equiv.) was added and stirred at 90 °C. After 24 h, the reaction mixture was cooled to RT and extracted with DCM (150 mL). The organic layer was then washed with water (100 mL × 3) and dried over anhydrous sodium sulfate. The crude mixture was purified by silica gel flash column chromatography using DCM:hexane = 2:8. The corresponding fractions were combined and concentrated under reduced pressure to afford a white solid, which was cooled at -20 °C for 2 h and filtered to obtain the product as a white solid (7.70 g). **Yield**: 95%. **R$_f$**: 0.28 (DCM:hexane = 20:80 on silica gel). **Mp**: 212-214 °C. **^{1}H NMR (500 MHz, CDCl$_3$)** δ 8.15 (d, J = 1.4 Hz, 2H), 7.51 (dd, J = 8.7, 1.7 Hz, 2H), 7.43 (dd, J = 8.5, 3.9 Hz, 3H), 7.35 – 7.23 (m, 3H), 7.12 (d, J = 8.3 Hz, 4H), 6.97 (d, J = 8.4 Hz, 4H), 6.94 (s, 2H), 2.45 (s, 3H), 2.32 (s, 6H), 1.52 (s, 18H). **^{13}C NMR (126 MHz, CDCl$_3$)** δ 157, 154, 143, 138, 138, 137, 133, 132, 130, 130, 127, 125, 123, 123, 123, 122,119, 116, 110, 109, 134, 32, 20, 20. **HR-MS [M]$^+$ Calculated:** (C$_{47}$H$_{48}$NO$_2$) 658.3685; **Found:** 658.3659.

2,11,14-trimethyl-6-(o-tolyl)-7-(p-tolyloxy)-5-oxa-8b-aza-15b-borabenzo[a]naphtho[1,2,3-hi]aceanthrylene (1B-Cz-Crs);   2,5,8,16-tetramethyl-12-(o-tolyl)-11,13-dioxa-3a2-aza-6b,17b-diboraindeno[4',3',2',1':3,4,5]phenanthro[2,1,10,9-fghi]pentacene (2B-Cz-Crs)
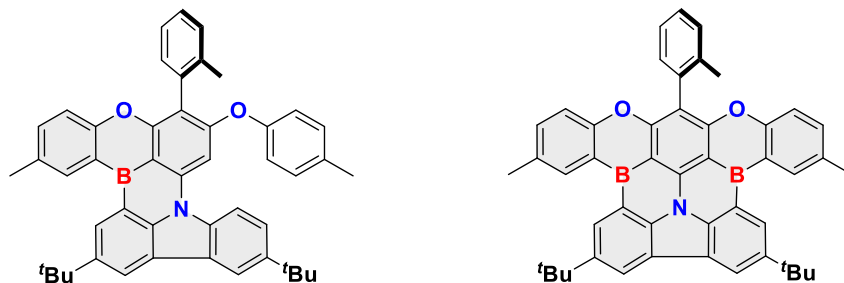
Compound **5** (1.5 g, 2.8 mmol, 1 equiv.), BI$_3$ (4.46 g, 11.4 mmol, 5.0 equiv.) and 2,6-di-*tert*-butylpyridine (1.53 mL, 6.84 mmol, 3.0 equiv.) were dissolved in 10 mL of 1,2,4-trichlorobenzene in a Schlenk under nitrogen at 0 °C. After stirring at 220 °C for 24 h, the cold reaction mixture was diluted with 150 mL of DCM. To this solution, 20 mL saturated 20% sodium acetate solution was added with stirring. The organic layer was then separated and washed with water (3 × 100 mL) followed by drying over anhydrous sodium sulfate. After concentrating the organic layer in vacuo, the crude product was dissolved in toluene (5 mL) and acetic acid (5 mL) at room temperature. After stirring at 80 °C for 18 h, saturated sodium carbonate (100 mL) was added to the reaction mixture, and then the aqueous layer was extracted with DCM (50 mL, 3×). The crude mixture was purified by silica gel flash column chromatography using DCM:hexane = 3:7; to afford **1B-CzCrs** (220 mg) (**Yield**: 15%) and **2B-CzCrs** (180 mg) (**Yield**: 12%) both as a yellow solid.

1B-CzCrs: **R$_f$:** 0.56 (DCM:hexane = 3:7 on silica gel). **Mp**: 269-271 °C. **^{1}H NMR (400 MHz, CD$_2$Cl$_2$)** δ 8.96 (d, J = 1.9 Hz, 1H), 8.63 – 8.57 (m, 1H), 8.47 (d, J = 1.8 Hz, 1H), 8.24 (d, J = 2.0 Hz, 1H), 7.75 (d, J = 9.2 Hz, 2H), 7.47 – 7.43 (m, 3H), 7.41 – 7.29 (m, 3H), 7.26 – 7.18 (m, 3H), 7.09 – 7.00 (m, 2H), 2.58 (s, 3H), 2.43 (s, 3H), 2.30 (s, 3H), 1.66 (s, 9H), 1.51 (s, 9H). **^{13}C NMR (101 MHz, CD$_2$Cl$_2$)** δ 160, 158, 157, 154, 144, 144, 142, 141, 138, 137, 134, 133, 133, 133, 131, 131, 130, 129, 129, 127, 126, 125, 124, 123, 120, 119, 117, 117, 114, 113, 113, 97, 35, 34 32, 31, 21, 20, 20. **Anal. Calcd. For C$_{47}$H$_{44}$BNO$_2$**: C, 84.80%; H, 6.66%; N, 2.10%. **Anal. Found**: C, 84.83%; H, 6.46%; N, 2.01. **HR-MS [M+H]$^+$ Calculated:** (C$_{47}$H$_{45}$BNO$_2$) 666.3543; **Found:** 666.3555. 99.7% pure on HPLC analysis, retention time 13.1 minutes in 75% THF 25% water.

2B-CzCrs: **R$_f$:** 0.48 (DCM:hexane = 3:7 on silica gel). **Mp**: > 290 °C. **^{1}H NMR (400 MHz, CD$_2$Cl$_2$)** δ 8.93 (d, J = 1.9 Hz, 2H), 8.61 (m, 2H), 8.55 (m, 2H), 7.60 – 7.58 (m, 1H), 7.49– 7.46 (m, 2H), 7.44 – 7.39 (m, 3H), 7.29 (s, 1H), 7.27 (s, 1H), 2.57 (s, 6H), 2.18 (s, 3H), 1.70 (s, 18H). **^{13}C NMR (101 MHz, CD$_2$Cl$_2$)** δ
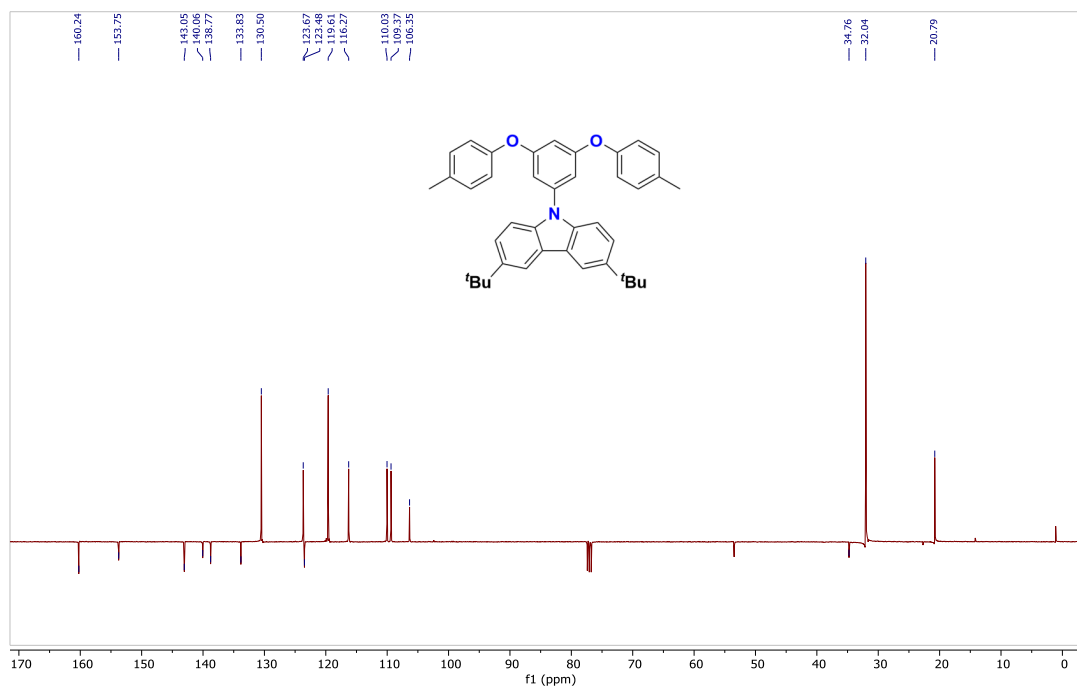
160, 158, 146, 140, 138, 138, 134, 133, 132, 132, 129, 129, 127, 125, 125, 124, 122, 120, 118, 109, 108, 34, 32, 21, 20. **Anal. Calcd. For C₄₂H₃₂N₂O₄**: C, 83.82%; H, 6.14%; N, 2.08%. **Anal. Found**: C, 82.27%; H, 5.09%; N, 1.84. **HR-MS [M+H]⁺ Calculated:** (C₄₇H₄₂B₂NO₂) 674.3402; **Found:** 674.3422. 99.1% pure on HPLC analysis, retention time 13.9 minutes in 75% THF 25% water.

Figure **S2**.¹H NMR (400 MHz, CDCl₃) spectrum of **3**.

Figure **S3**. [13] DEPTq-135 (101 MHz, CDCl$_3$) spectrum of **3**.
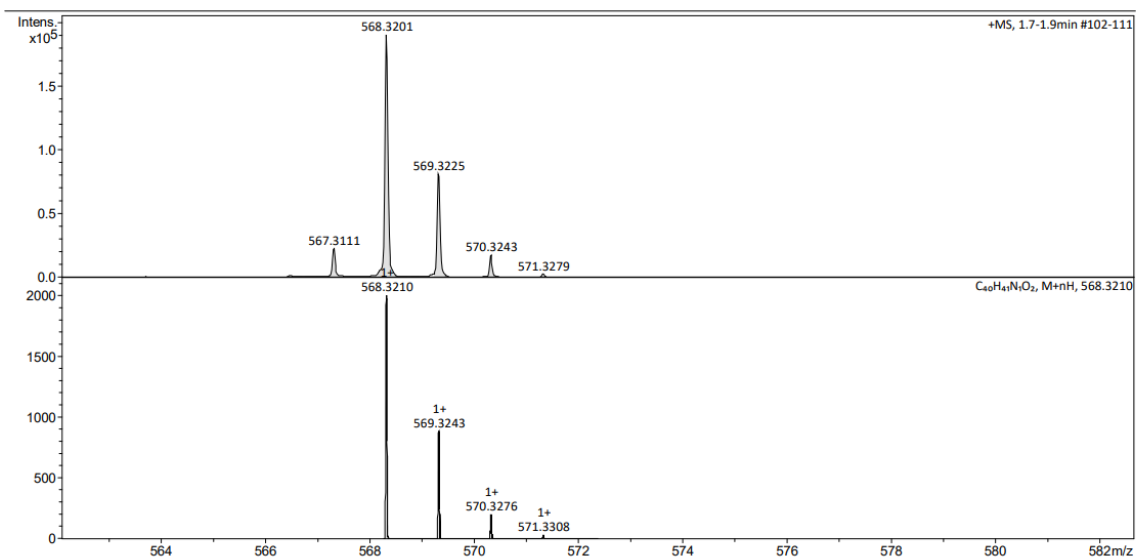
Figure **S4**. HRMS of compound **3**.
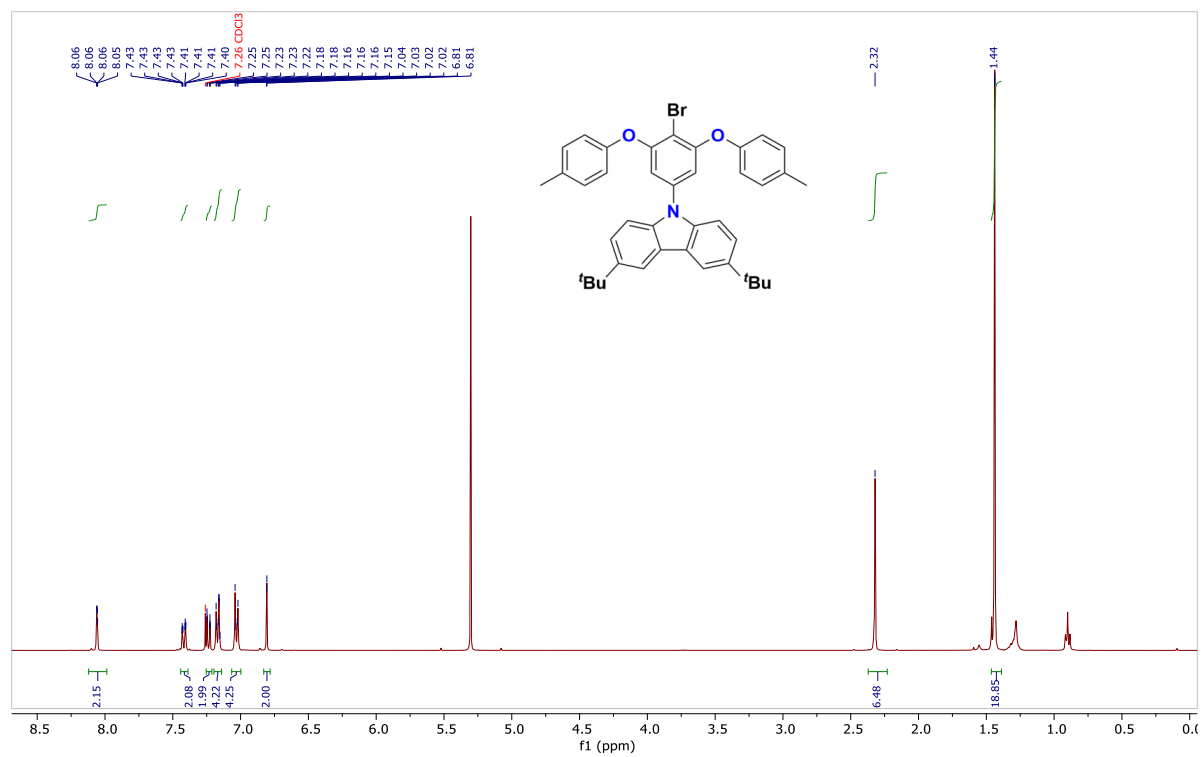
Figure **S5**. ¹H NMR (400 MHz, CDCl₃) spectrum of **4**.
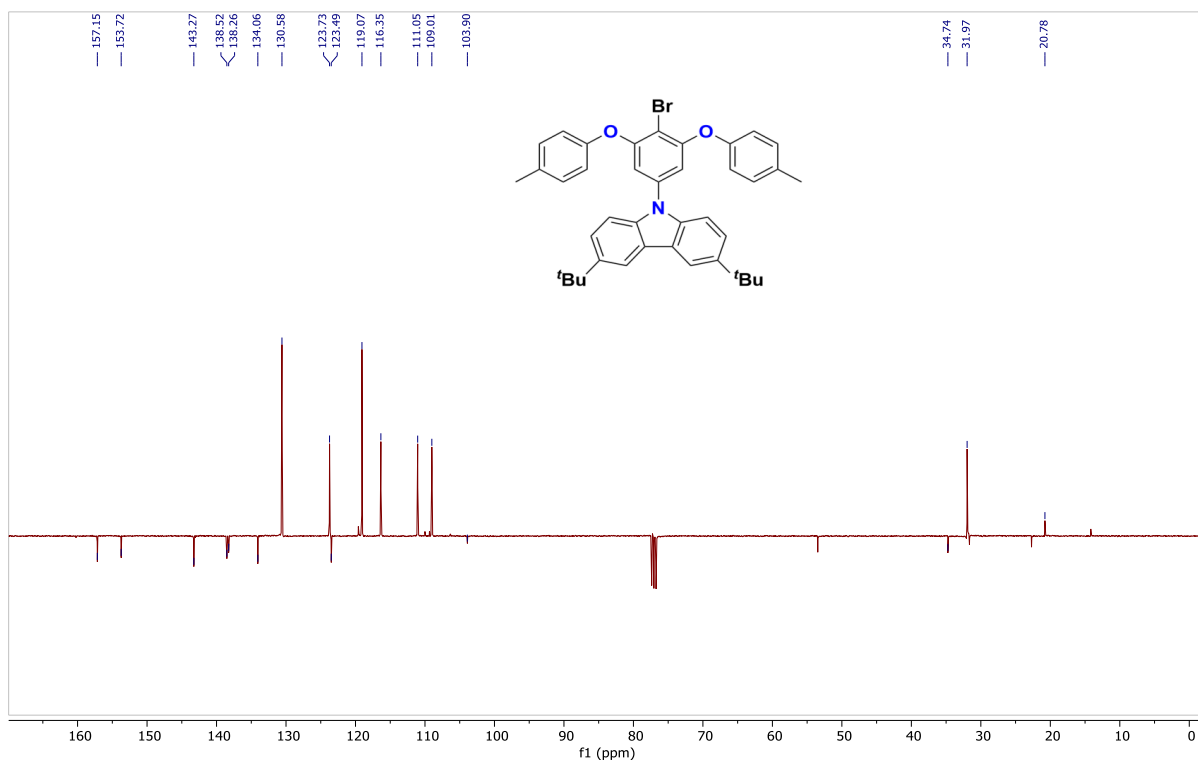
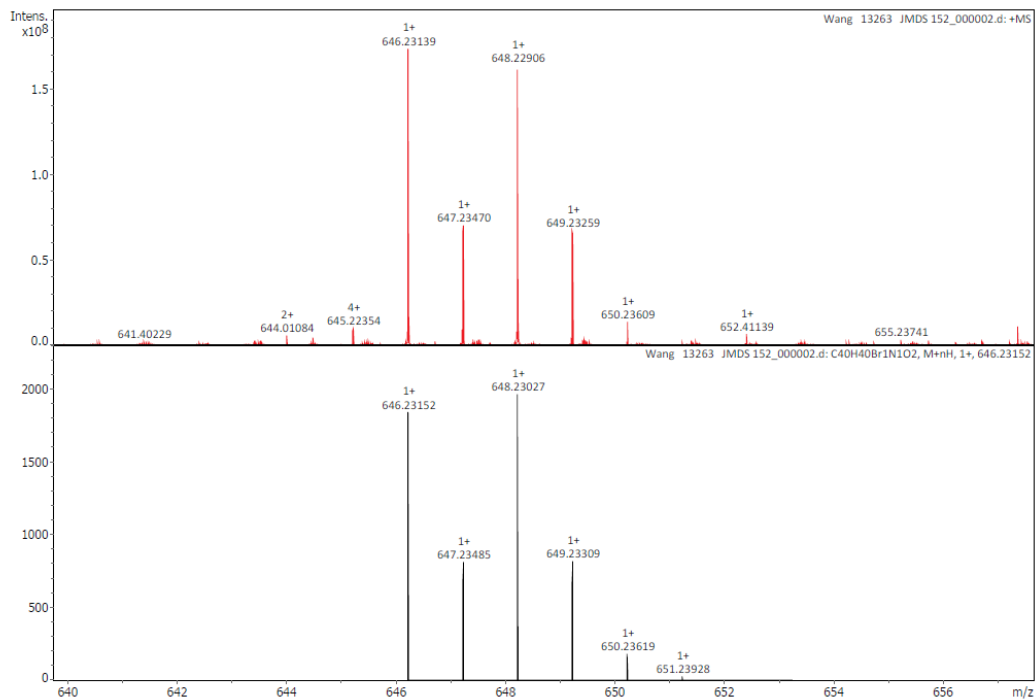Figure **S6**. DEPTq-135 (101 MHz, CDCl₃) spectrum of **4**.
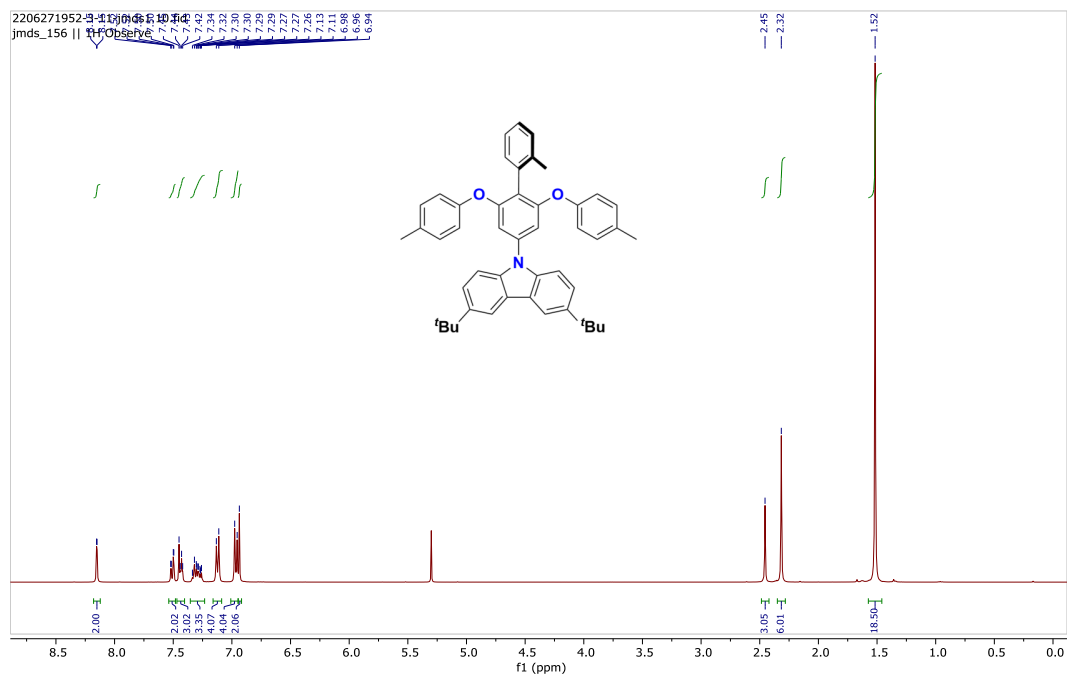
Figure **S7.** HRMS of compound **4**.

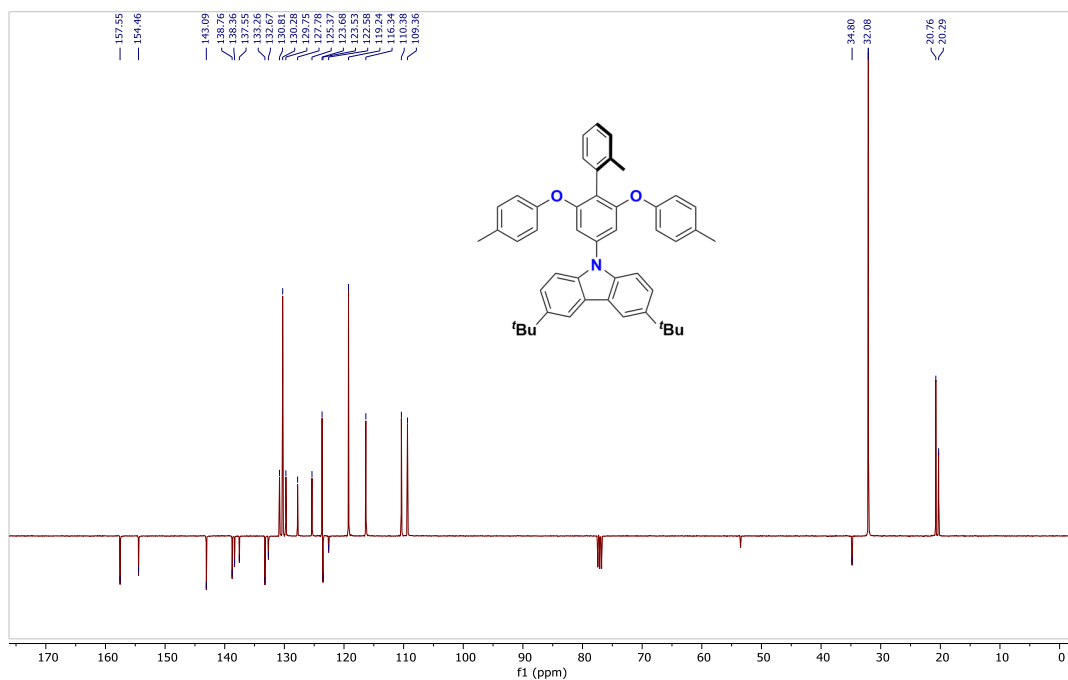Figure **S8**. ^{1}H NMR (400 MHz, CDCl$_3$) spectrum of **3**.

Figure **S9**. DEPTq-135 (126 MHz, CDCl₃) spectrum of **5**.
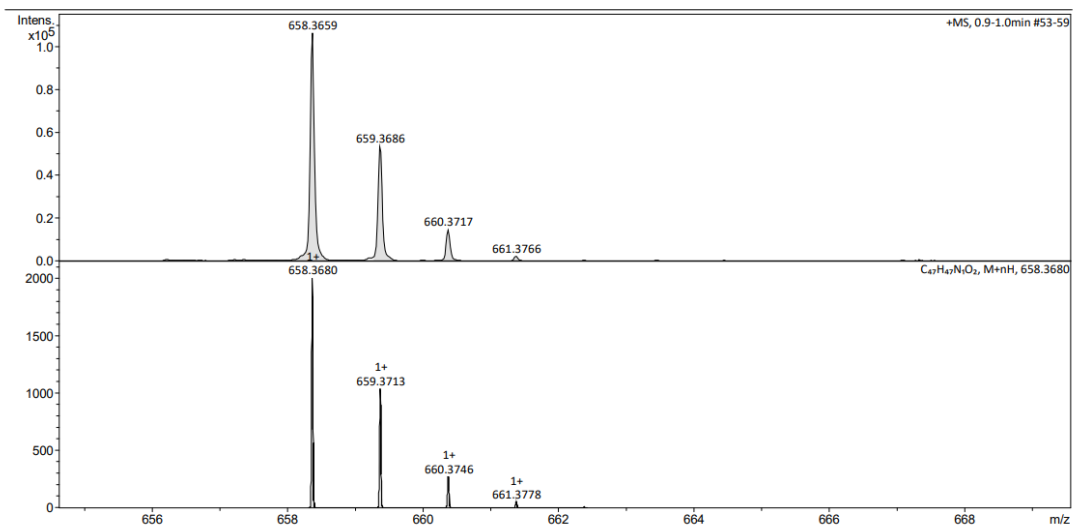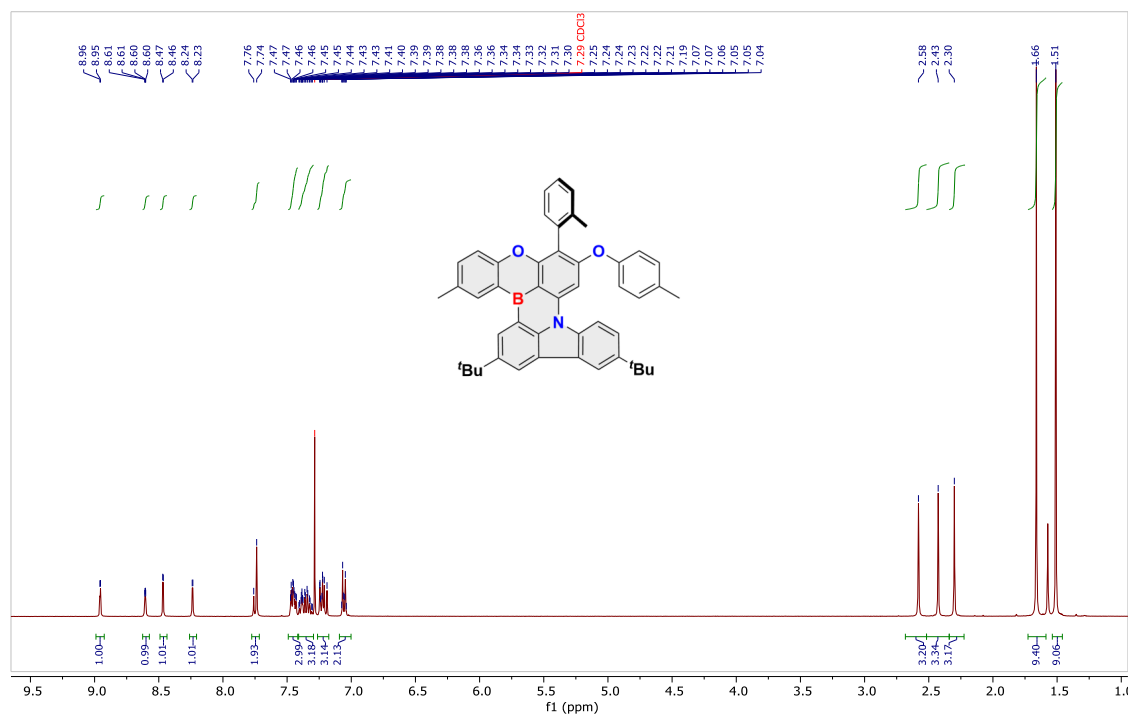

Figure **S10**. HRMS of compound **5**.

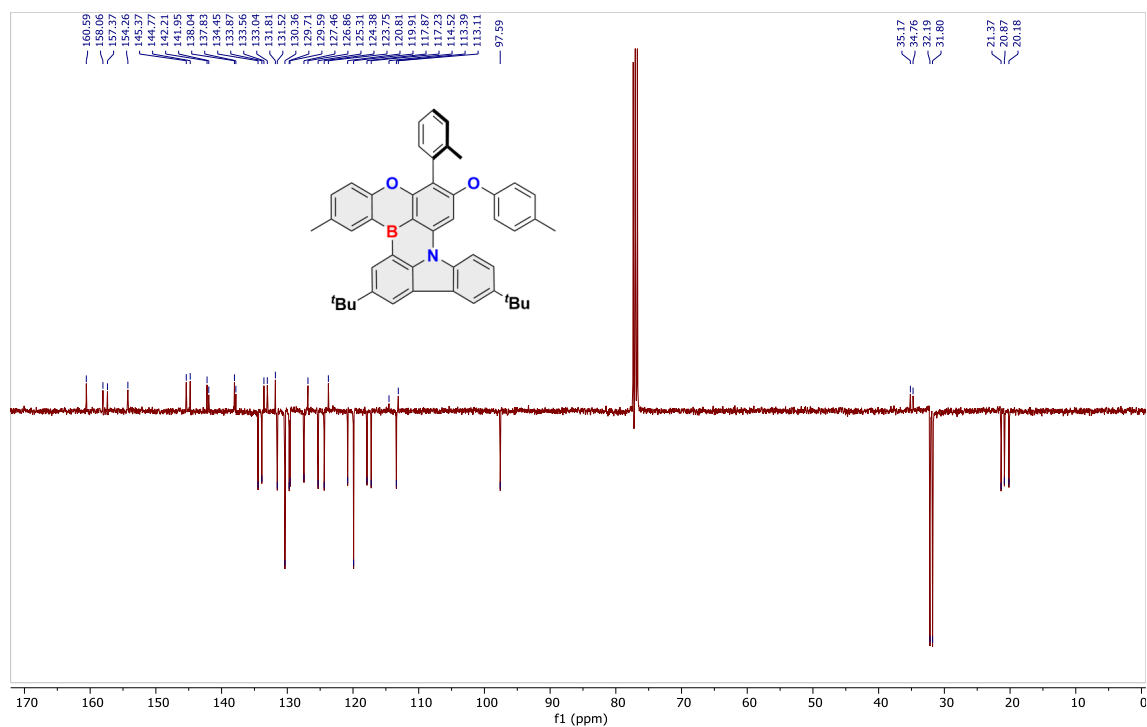Figure **S11**. ^{1}H NMR (400 MHz, CDCl$_3$) spectrum of **1B-CzCrs**.

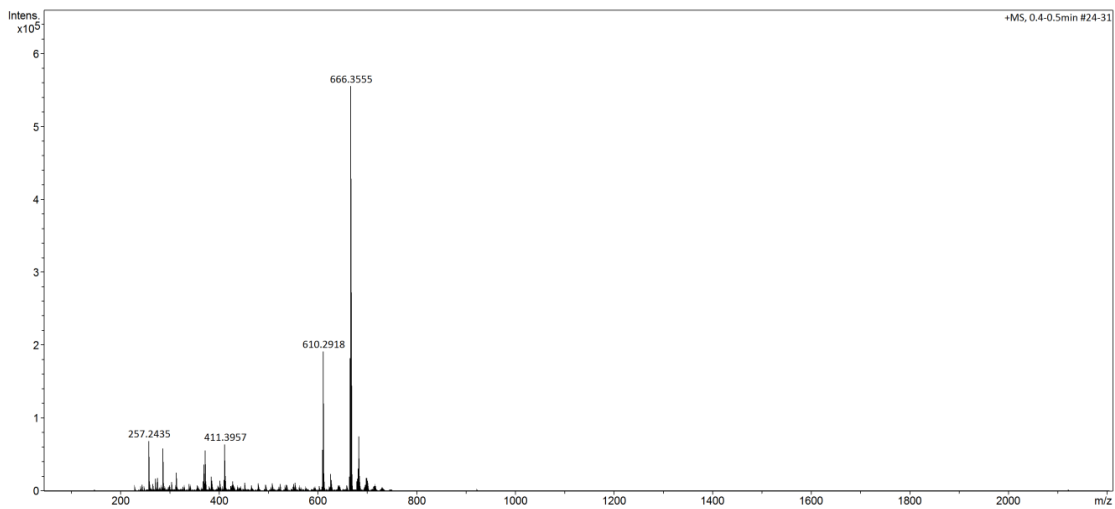Figure **S12**. DEPTq-135 (101 MHz, CDCl$_3$) spectrum of **1B-CzCrs**.

Figure **S13**. HRMS of compound **1B-CzCrs**.
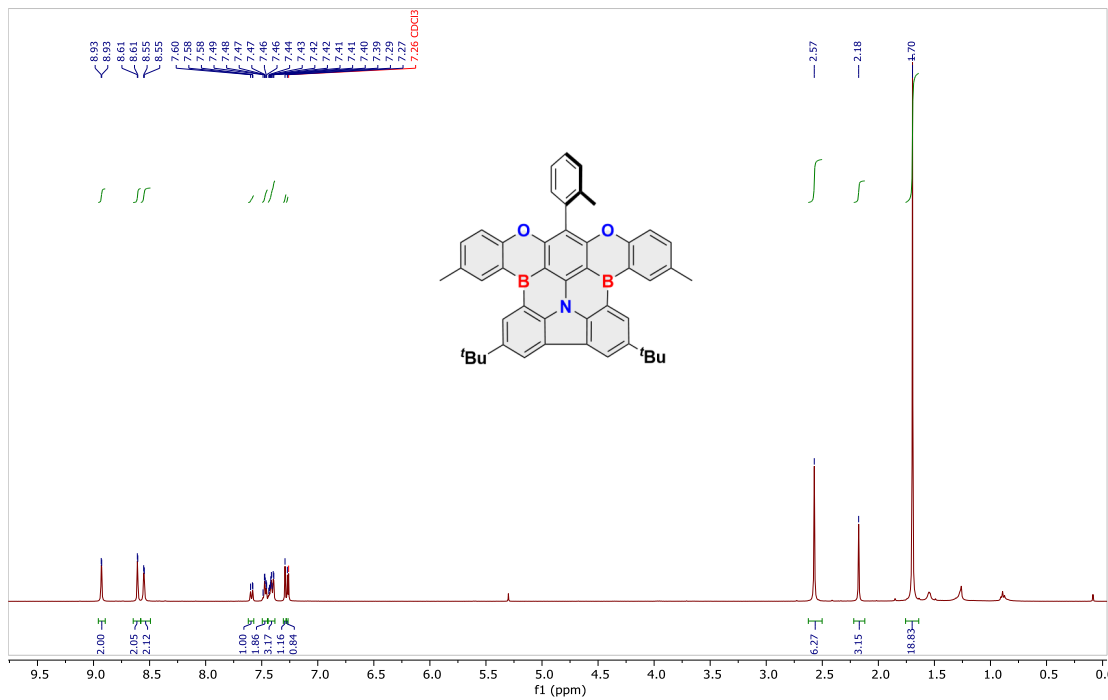

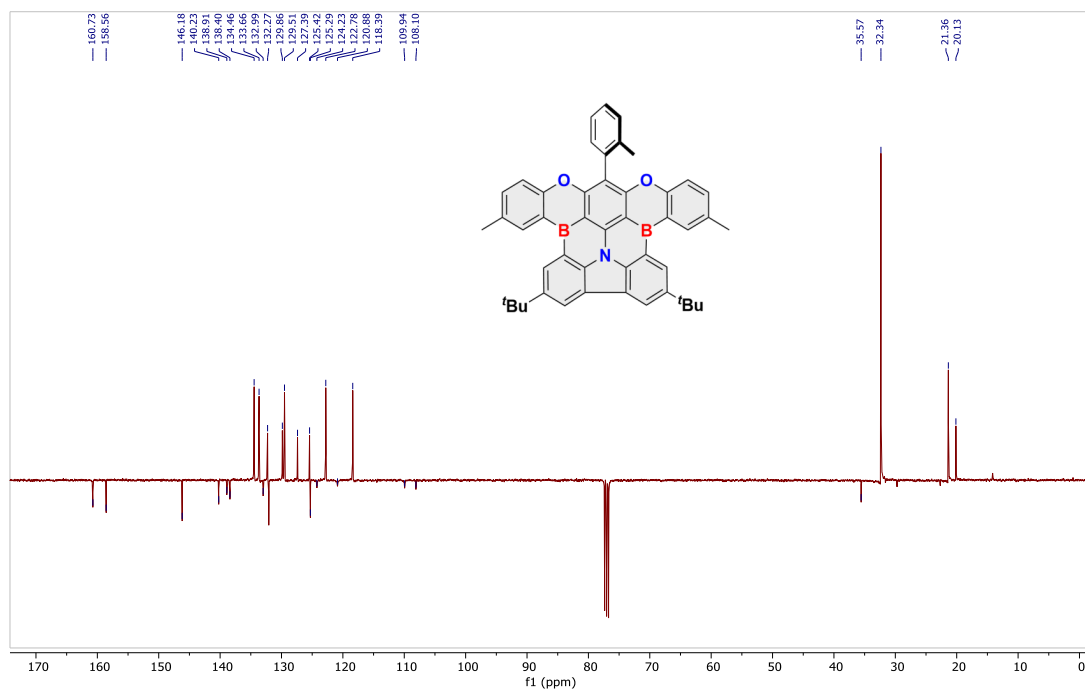Figure **S14**. ^{1}H NMR (400 MHz, CDCl$_3$) spectrum of **2B-CzCrs**.

S15

Figure **S15**. DEPTq-135 (101 MHz, CDCl₃) spectrum of **2B-CzCrs**.
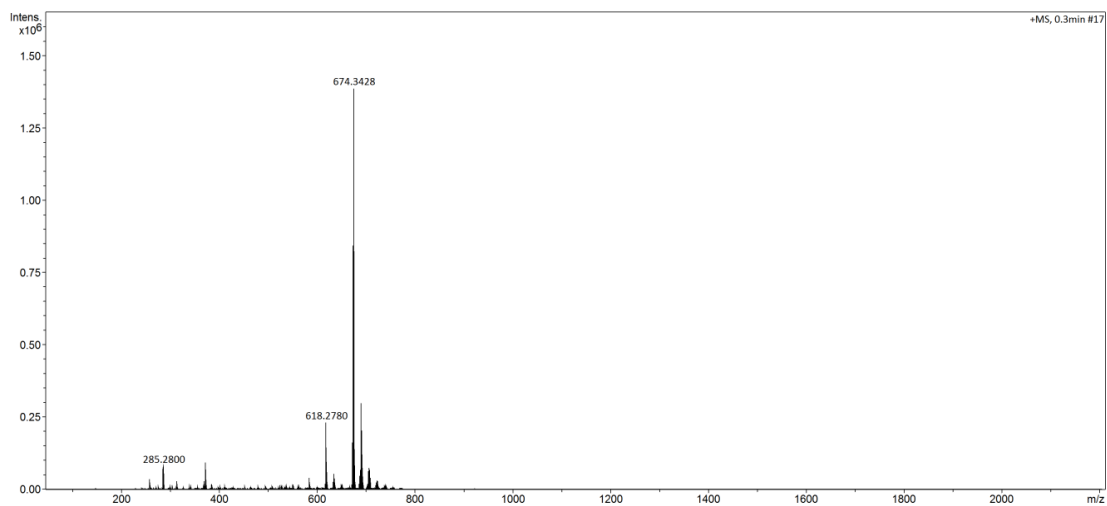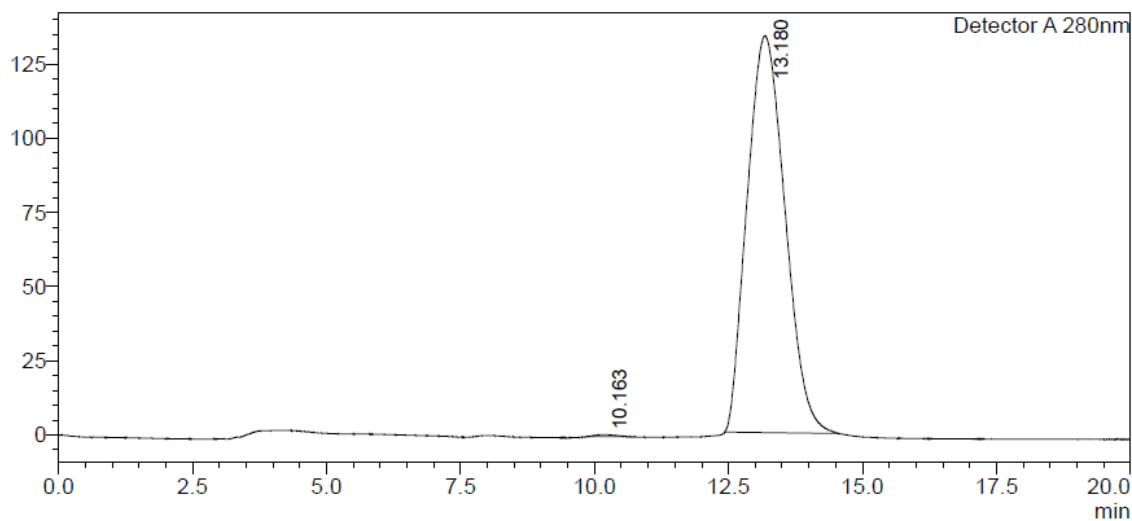

Figure **S16**. HRMS of compound **2B-CzCrs**.

<Peak Table>

Detector A 280nm

Peak#	Ret. Time	Area	Height	Area%	Area/Height	Width at 5% Height
1	10.163	19109	650	0.289	29.389	0.829
2	13.180	6589289	133749	99.711	49.266	1.540
Total		6608399	134400	100.000		

Figure **S17**. HPLC trace of **1B-CzCrs**.

<Peak Table>
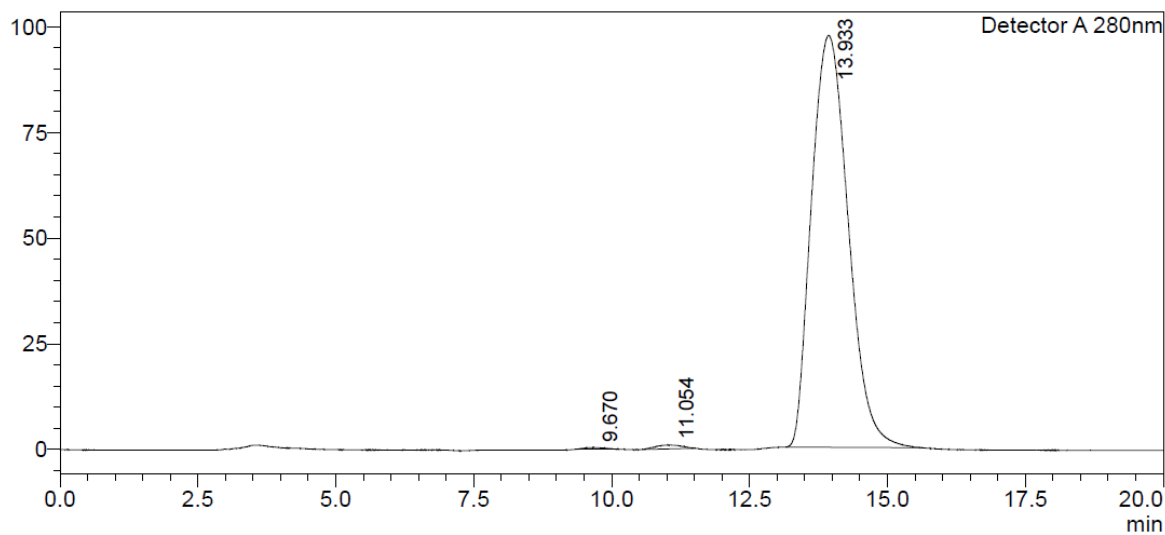
Detector A 280nm

Peak#	Ret. Time	Area	Height	Area%	Area/Height	Width at 5% Height
1	9.670	10229	391	0.225	26.153	0.711
2	11.054	29624	897	0.651	33.028	0.894
3	13.933	4512316	97386	99.125	46.334	1.461
Total		4552169	98674	100.000		

Figure **S18**. HPLC trace of **2B-CzCRs**.

3. Electrochemistry

Figure **S19**. Cyclic and differential pulse voltammograms (CV and DPV) of (a) **1B-CzCrs** and (b) **2B-CzCrs**, measured in degassed D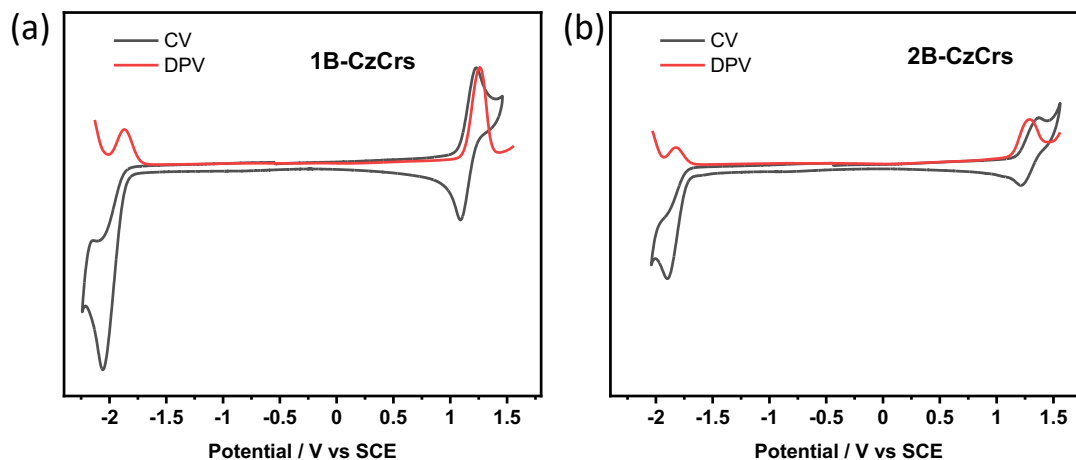CM with 0.1 M $^nBu_4NPF_6$ as the supporting electrolyte and Fc/Fc$^+$ as the external reference (0.46 V vs SCE);[19] Scan rate = 100 mV s^{-1}.

Table **S2**. Electrochemical data of **1B-CzCrs** and **2B-CzCrs**.

Compound	E_{ox} [a] / V	E_{red} [a] / V	HOMO [b] / eV	LUMO [b] / eV	ΔE [c] / eV
1B-CzCrs	0.80	-2.33	-5.60	-2.47	3.13
2B-CzCrs	0.82	-2.28	-5.62	-2.52	3.10
1B-DTACrs [d]	1.07	-2.10	-5.42	-2.24	3.17
2B-DTACrs [d]	1.17	-1.89	-5.51	-2.46	3.05

[a] Potential values obtained from the DPV peak values, measured in degassed dichloromethane with 0.1 M $^nBu_4NPF_6$ as the supporting electrolyte and referenced with respect to SCE (Fc/Fc$^+$ = 0.46 eV).[19] [b] HOMO and LUMO energy levels determined using the relation $E_{HOMO}/_{LUMO} = -(E_{ox}/E_{red} + 4.6)$ eV (using Fc/Fc$^+$ as the external reference);[14] [c] $\Delta E = |HOMO-LUMO|$ eV. [d] Reported values from the literature.[21]

4. Thermal gravimetric analysis

(a)

(b)
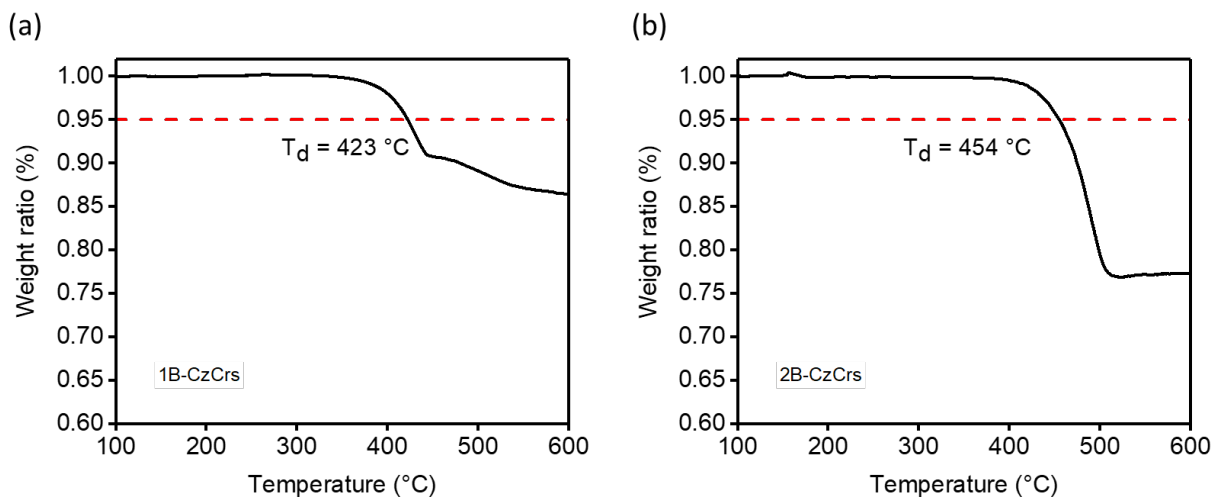
Figure **S20**. Thermal stability of **1B-CzCrs** (a) and **2B-CzCrs** (b) determined by thermogravimetric analysis (the decomposition temperature, T_d determined from the temperature at 5 wt% mass loss).

5. Theoretical Calculations and Photophysical Properties

Table **S3**. HOMO, LUMO, and E_g values of **1B-CzCrs**, **2B-CzCrs**, and **1B-DTACrs**.

Compound	HOMO (eV)	LUMO (eV)	E_g (eV)
1B-CzCrs	-5.39	-1.51	3.77
2B-CzCrs	-5.47	-1.69	3.88
1B-DTACrs [a]	-5.27	-1.24	4.03
2B-DTACrs [a]	-5.38	-1.47	3.91

[a] Reported values from the literature.[21]

Table **S4**. Estimated S_1, T_1, T_2, and ΔE_{ST} values for **1B-CzCrs**, **2B-CzCrs**, and **1B-DTACrs** using different calculation methods in the gas phase.

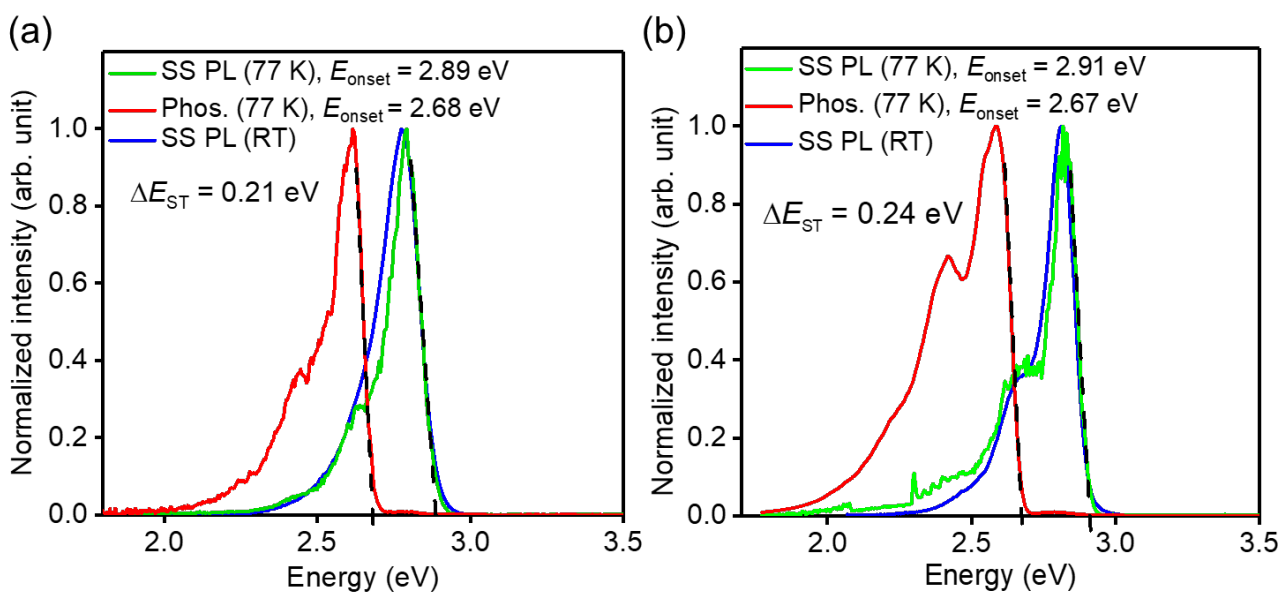|	at SCS-CC2/cc–pVDZ			at TDADFT-PBE0/6-31G**		
	1B-CzCrs (eV)	2B-CzCrs (eV)	1B-DTACrs [a] (eV)	1B-CzCrs (eV)	2B-CzCrs (eV)	1B-DTACrs (eV)
S_1	3.00	3.00	3.38	3.11	3.03	3.24
T_1	2.84	2.83	3.18	2.78	2.62	2.69
T_2	3.29	3.02	3.72	2.99	2.95	3.42
$\Delta E_{S1\text{-}T1}$	0.16	0.17	0.2	0.33	0.40	0.55
$\Delta E_{S1\text{-}T2}$	-0.29	-0.02	-0.34	0.13	0.08	-0.18

[a] Reported values in literature.[21]

Figure **S21**. Energy scale representation[16] of steady-state (SS) PL at RT and 77 K and phosphorescence spectra (delay: 115 ms, gate: 150 ms) for (a) **1B-CzCrs** and (b) **2B-CbzCrs** in toluene. (λ_{exc} = 310 nm).
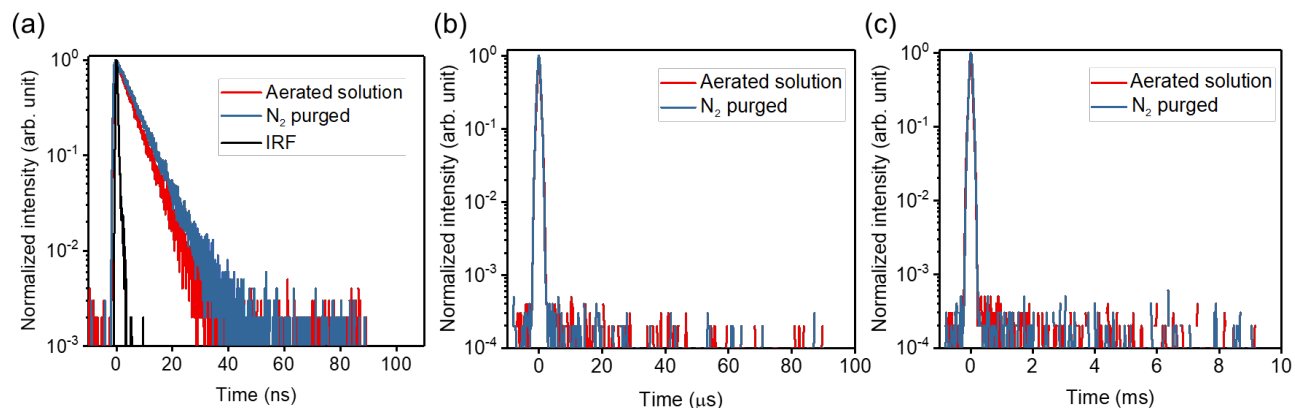
Figure **S22**. Transient decays of **1B-CzCrs** in toluene at (a) 100 ns, (b) 100 μs, and (c) 10 ms time ranges under aerated (red) and N_2-purged (blue) conditions. (Prompt time range measurements (100 ns) were taken with Quanturus-Tau at λ_{exc} = 340 nm, while 100 μs and 10 ms range measurements were taken using the Streak camera measurement system at λ_{exc} = 355 nm).

Figure **S23**. Transient decays of **2B-CzCrs** in toluene at (a) 100 ns, (b) 100 μs, and (c) 10 ms time ranges under aerated (red) and N_2-purged (blue) conditions. (Prompt time range measurements (100 ns) were taken with Quanturus-Tau at λ_{exc} = 340 nm, while 100 μs and 10 ms range measurements were taken using the Streak camera measurement system at λ_{exc} = 355 nm).
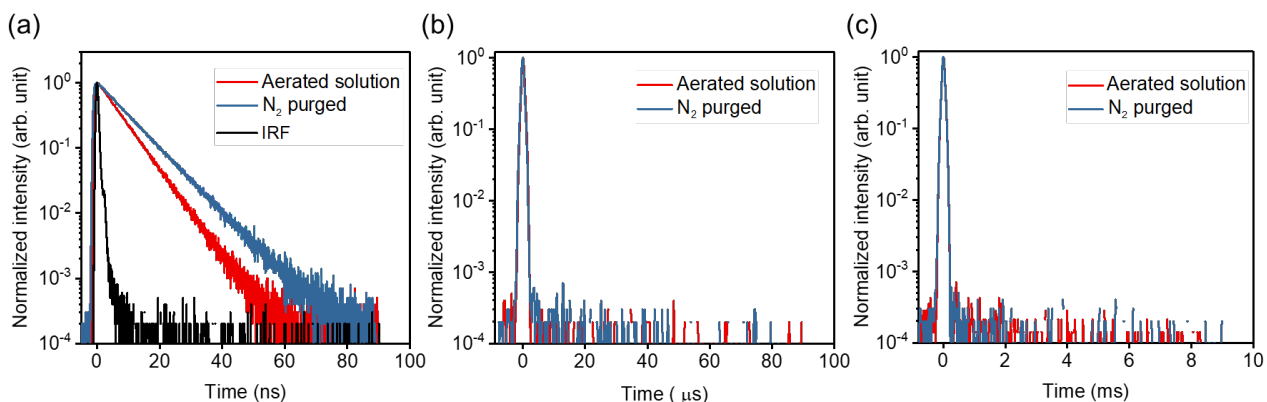
Table **S5**. Photophysical data of 5 wt% doped **1B-CzCrs**, **2B-CzCrs**, **1B-DTACrs,** and **2B-DTACrs** in **mCBP** host**.**

Emitter	$\Phi_{PL_{(Ar)}}$ [a] (%)	λ_{PL} [b] (nm)	S_1 [c] (eV)	T_1 [d] (eV)	ΔE_{ST} [c,d] (eV)	FWHM (nm)	τ_p [e] (ns)	τ_d [e] (ms)	k_{RISC} (10^3 s^{-1})
1B-CzCrs	67	451	2.89	2.69	0.20	28	5.08	0.33	3.36
2B-CzCrs	59	449	2.91	2.67	0.24	28	8.63	2.98	0.41
1B-DTACrs [f]	83	443	-	-	0.21	28	10	-	-
2B-DTACrs [f]	74	448	-	-	0.16	24	2	0.013	130.0

[a] Absolute Φ_{PL} of thin films was measured using an integrating sphere. [b] Fluorescence maximum at RT (λ_{exc}=310 nm). [c] Obtained from the onset of the PL spectrum at 77 K. [d] Obtained from the onset of the phosphorescence at 77 K (delay 115 ms, gate 150 ms, λ_{exc} = 310 nm). [e] Observed at emission peak wavelength. [f] Reported values from the literature.[21]
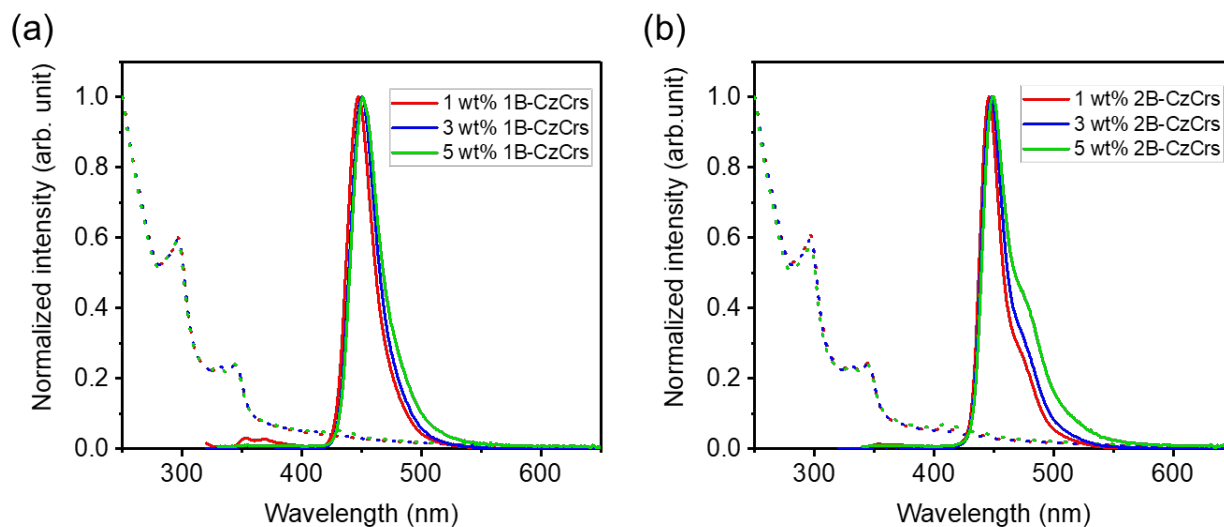

Figure **S24**. Absorption (dotted lines) and fluorescence (solid lines) spectra of (a) **1B-CzCrs** and (b) **2B-CzCrs** doped **mCBP** films at the various concentrations (λ_{exc}= 310 nm).
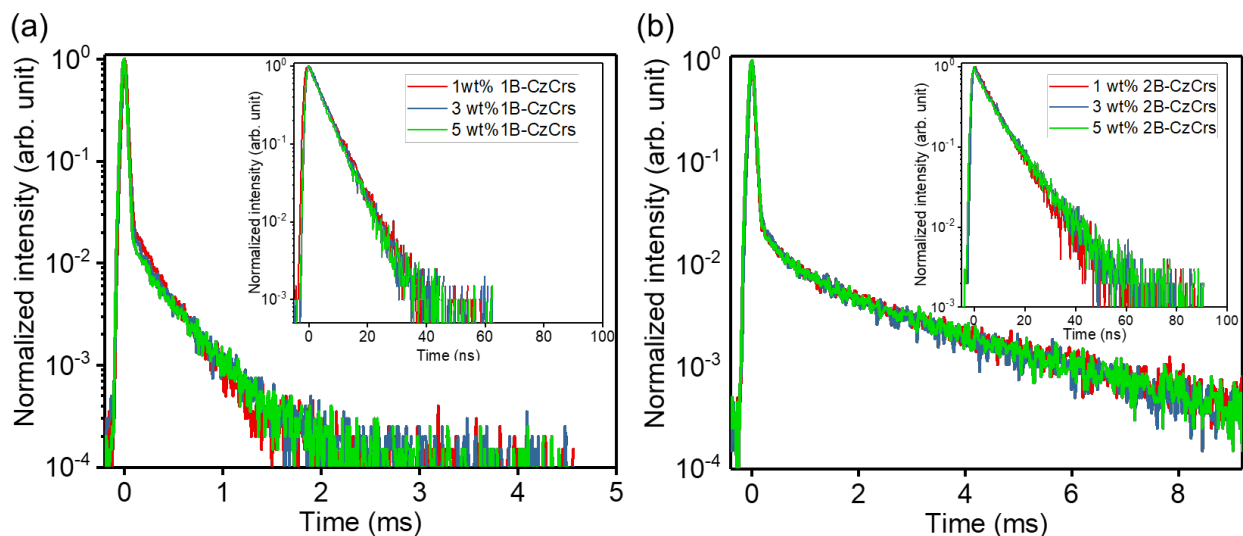
Figure **S25**. Time-resolved PL decays of (a) **1B-CzCrs** and (b) **2B-CzCrs** doped **mCBP** films at various concentrations. Insets: Prompt PL decay curves (λ_{exc}= 355 nm).

Table **S6**. Photophysical data of 1, 3, and 5 wt% doped films of **1B-CzCrs** and **2B-CzCrs** in **mCBP** host and the corresponding CIE coordinate values.

Emitter	wt%	$\Phi_{PL(Ar)}$ [a] (%)	λ_{PL} [b] (nm)	FWHM (nm)	CIE (x,y)	τ_p [c] (ns)	τ_d [c] (ms)
1B–CzCrs	1	76	447	25	0.151, 0.037	5.44	0.274
	3	83	450	26	0.148, 0.043	5.13	0.308
	5	67	451	28	0.151, 0.065	5.05	0.329
2B–CzCrs	1	87	446	20	0.149, 0.043	7.79	2.61
	3	73	448	23	0.147, 0.053	8.24	2.70
	5	59	449	28	0.150, 0.088	8.63	2.88

[a] Absolute Φ_{PL} of thin films was measured using an integrating sphere at λ_{exc}=340 nm. [b] Fluorescence maximum at RT (λ_{exc}=310 nm). [c] Under vacuum condition (λ_{exc} = 355 nm).

Table **S7**. Estimated SOC values for **1B-CzCrs**, **2B-CzCrs**, and **1B-DTACrs** based on each optimized geometry by TDA-DFT with PBE0/6-31G(d,p) level of theory.

	S_0 optimized		S_1 optimized		T_1 optimized		T_2 optimized	
	$\langle S_1\|H_{SOC}\|T_1\rangle$ (cm⁻¹)	$\langle S_1\|H_{SOC}\|T_2\rangle$ (cm⁻¹)	$\langle S_1\|H_{SOC}\|T_1\rangle$ (cm⁻¹)	$\langle S_1\|H_{SOC}\|T_2\rangle$ (cm⁻¹)	$\langle S_1\|H_{SOC}\|T_1\rangle$ (cm⁻¹)	$\langle S_1\|H_{SOC}\|T_2\rangle$ (cm⁻¹)	$\langle S_1\|H_{SOC}\|T_1\rangle$ (cm⁻¹)	$\langle S_1\|H_{SOC}\|T_2\rangle$ (cm⁻¹)
1B-CzCrs	0.0374	0.1342	0.0640	0.1315	0.1187	0.0995	0.1187	0.0995
2B-CzCrs	0.0000	0.0592	0.0000	0.1005	0.0592	0.0600	0.0500	0.1005
1B-DTACrs	0.0748	0.4730	0.0671	0.3750	0.0458	0.3746	0.0458	0.3746
2B-CzCrs	0.0300	0.9111	0.1217	08810	0.3713	0.8108	0.37135	0.8108

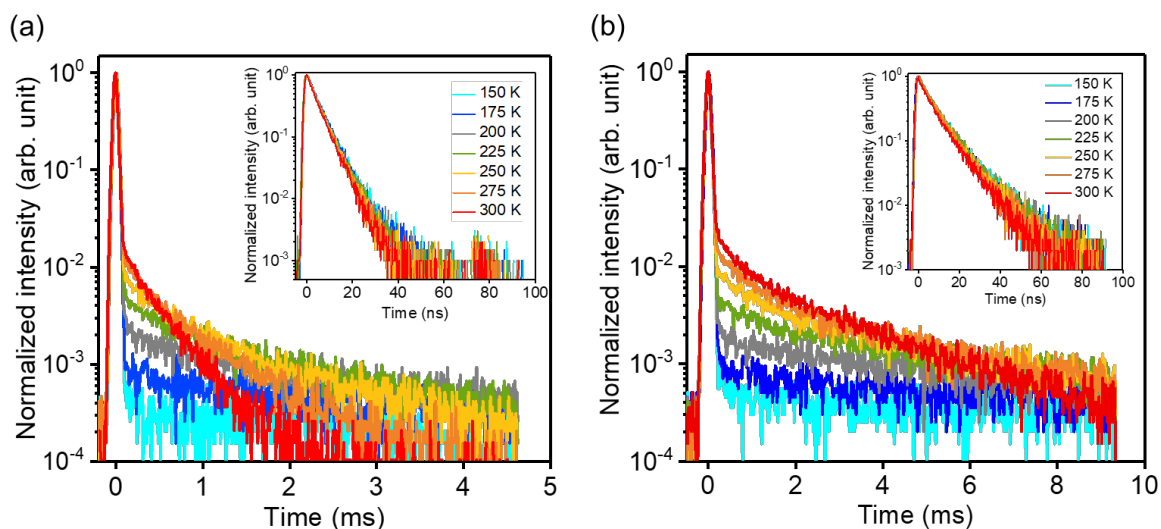Figure **S26.** Temperature-dependent transient PL decays of 5 wt% of (a) **1B-CzCrs**, (b) **2B-CzCrs** in **mCBP** under vacuum; insets, prompt PL decay curves (λ_{exc} = 355 nm).
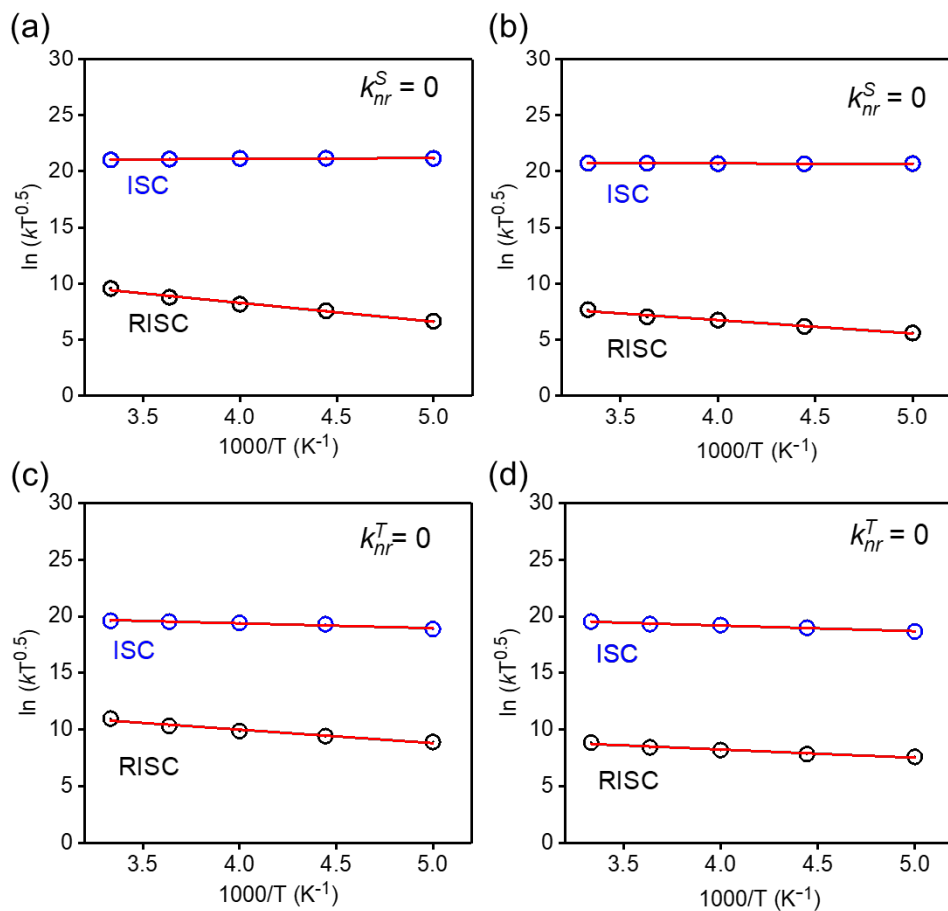

Figure **S27**. Marcus plots (for ISC and RISC) for 5 wt% doped films of **1B -CzCrs** (a, c) and **2B-CzCrs** (b, d) in **mCBP**, at the limit conditions of $k_{nr}^S = 0$ (a, b) and $k_{nr}^T = 0$ (c, d).

Table **S8**. Results of Marcus analysis for 5 wt% doped films of **1B-CzCrs** and **2B-CzCrs** in **mCBP.**

	E_a^{ISC} (meV)		E_a^{RISC} (meV)		ΔE_{ST} [a] (meV)		Effective SOCME [b] (cm^{-1})	
	$k_{nr}^S = 0$	$k_{nr}^T = 0$	$k_{nr}^S = 0$	$k_{nr}^T = 0$	$k_{nr}^S = 0$	$k_{nr}^T = 0$	$k_{nr}^S = 0$	$k_{nr}^T = 0$
1B–CzCrs	-6.4	36.7	145.1	102.5	151.5	65.9	0.0181	0.0173
2B–CzCrs	2.4	43.1	102.8	63.0	100.4	19.9	0.0029	0.0027

[a] $\Delta E_{ST} = E_a^{\text{RISC}} - E_a^{\text{ISC}}$, [b] $SOCME = \sqrt{e^{\ln\beta}\hbar(4\pi\lambda k_B)^{0.5}/2\pi}$ where β is intercept of Marcus plot for k_{RISC}, $\hbar$ is Dirac constant, λ is reorganization energy provided by $E_a^{\text{ISC}} + E_a^{\text{RISC}} + 2\sqrt{E_a^{\text{ISC}}E_a^{\text{RISC}}}$ (assuming under Marcus's normal region), and k_B is Boltzmann constant.[17, 18]
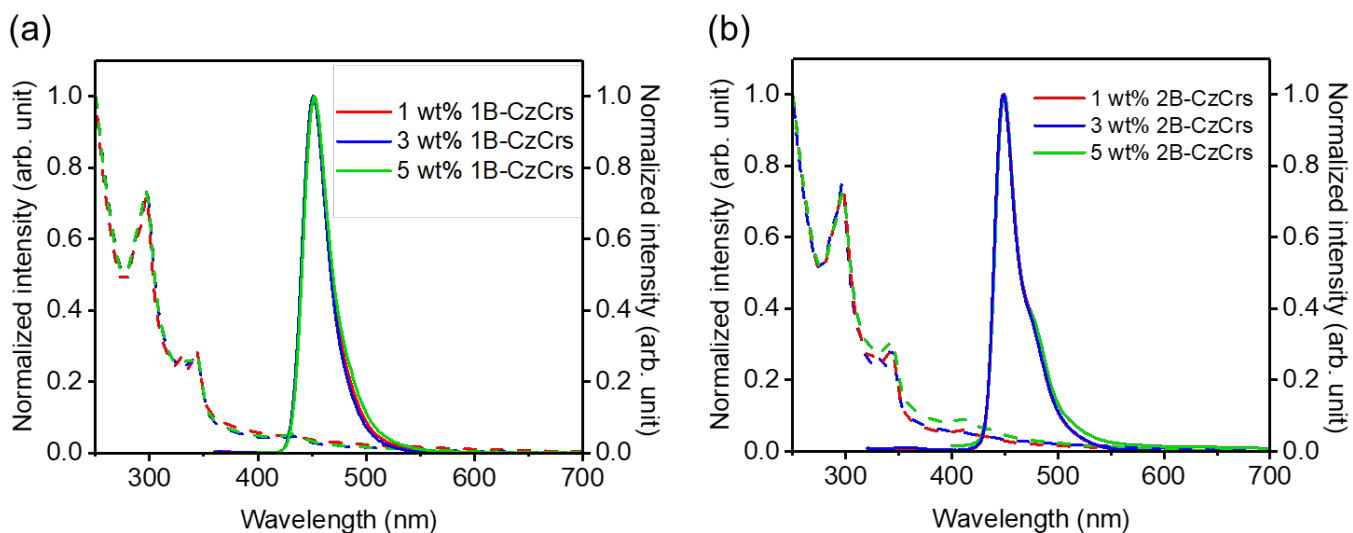

Figure **S28**. Steady-state absorption (dashed lines) and PL spectra (solid lines) of (a) **1B-CzCrs** and (b) **2B-CzCrs** at different doping concentrations in **mCP**. (λ_{exc} = 310 nm).
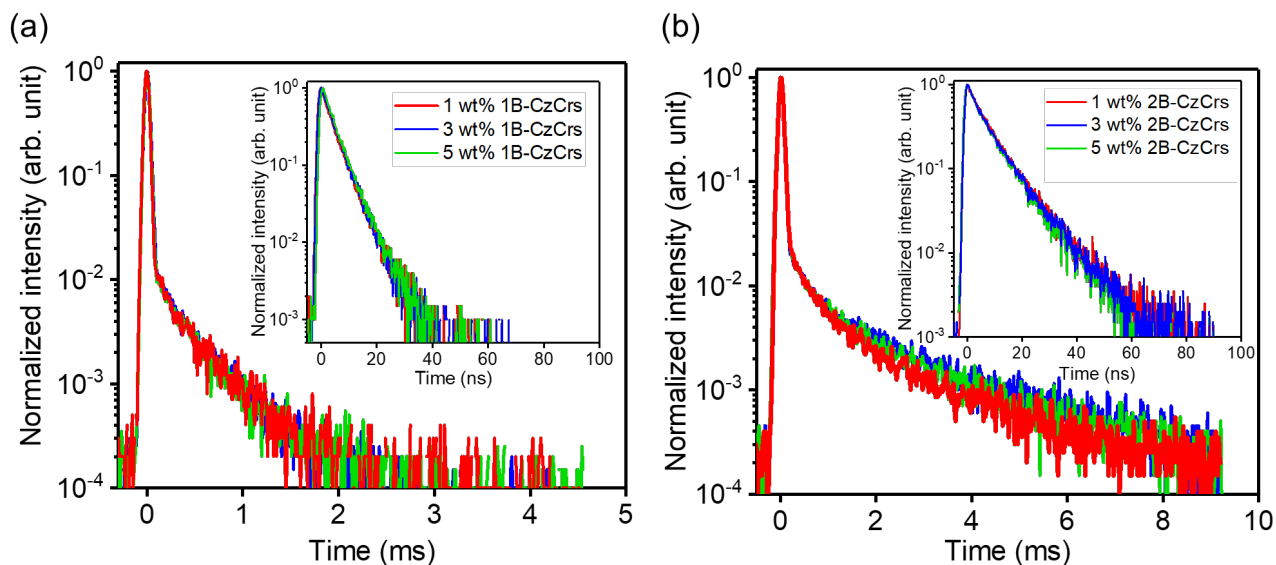
Figure **S29**. PL decays of (a) **1B-CzCrs** and (b) **2B-CzCrs** at different doping concentrations in **mCP**. Insets: Prompt PL decay curves. (λ_{exc} = 355 nm)

Table **S9**. Steady-state photophysical properties of **1B-CzCrs** and **2B-CzCrs** at different doping concentrations in **mCP** host and the corresponding CIE coordinates.

Emitter	wt%	$\Phi_{PL(Ar)}$ [a] (%)	λ_{PL} [b] (nm)	FWHM (nm)	CIE (x,y)	τ_p [c] (ns)	τ_d [c] (ms)
	1	72	451	28	0.146, 0.054	4.63	0.389
1B-CzCrs	3	79	451	28	0.145, 0.052	4.65	0.362
	5	75	452	29	0.145, 0.063	4.58	0.383
	1	65	448	25	0.141, 0.056	8.87	1.76
2B-CzCrs	3	64	448	25	0.144, 0.060	8.85	2.01
	5	62	449	26	0.145, 0.062	8.71	1.86

[a] Absolute Φ_{PL} of thin films was measured using an integrating sphere at λ_{exc} = 340 nm. [b] Fluorescence maximum at RT. (λ_{exc} = 310 nm). [c] Under vacuum condition (λ_{exc} = 355 nm).
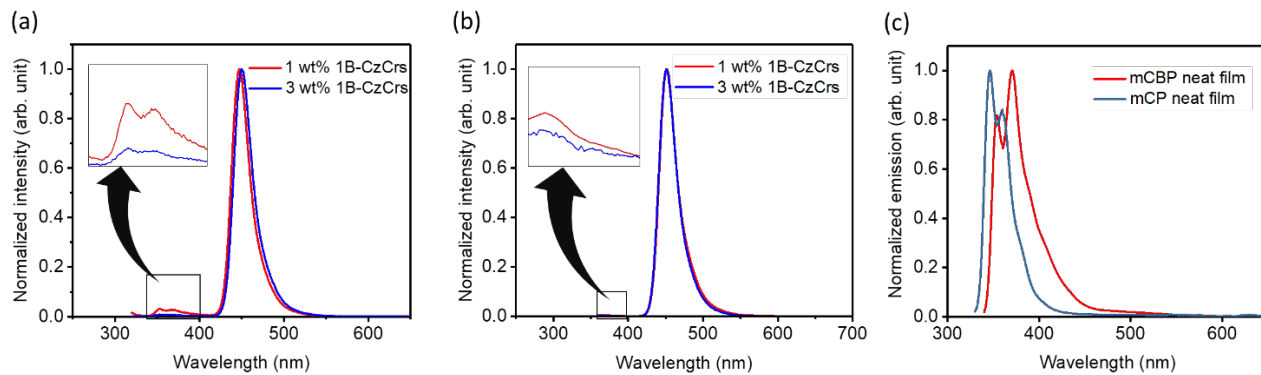
Figure **S30**. The emission profiles of 1 wt% (red line) and 2 wt% (blue line) of **1B-CzCrs** in different hosts; (a) **mCBP** and (b) **mCP**. (c) PL spectra of the **mCBP** (red line) and **mCP** neat films (blue line).
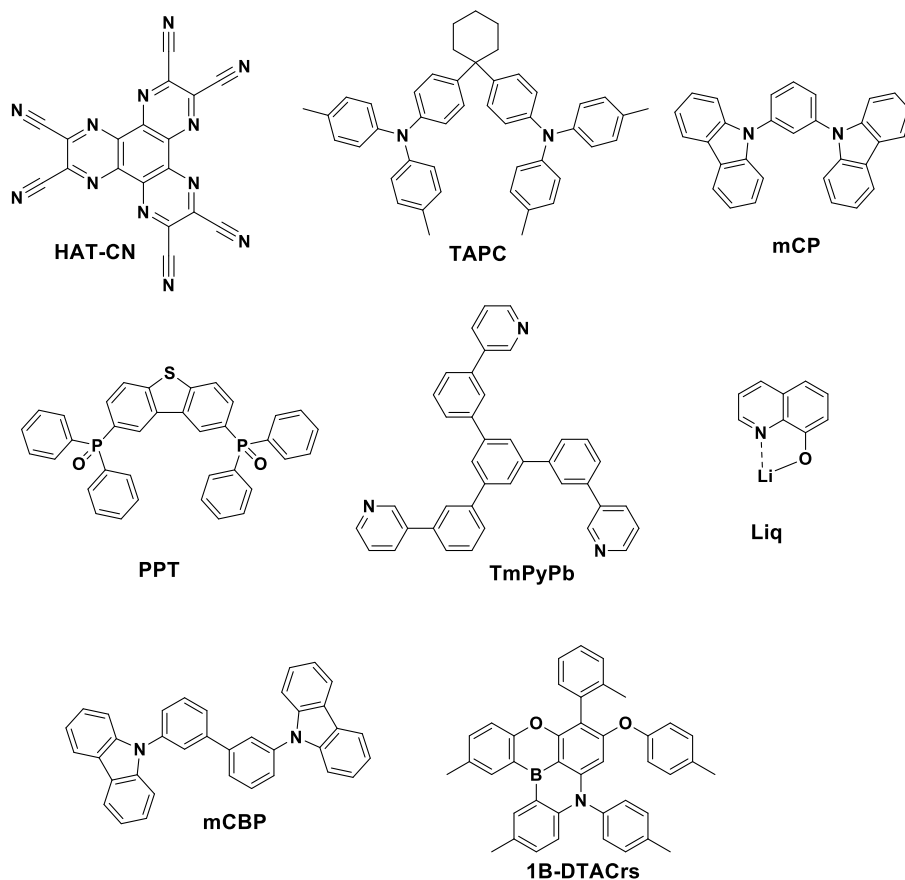
6. Device Properties

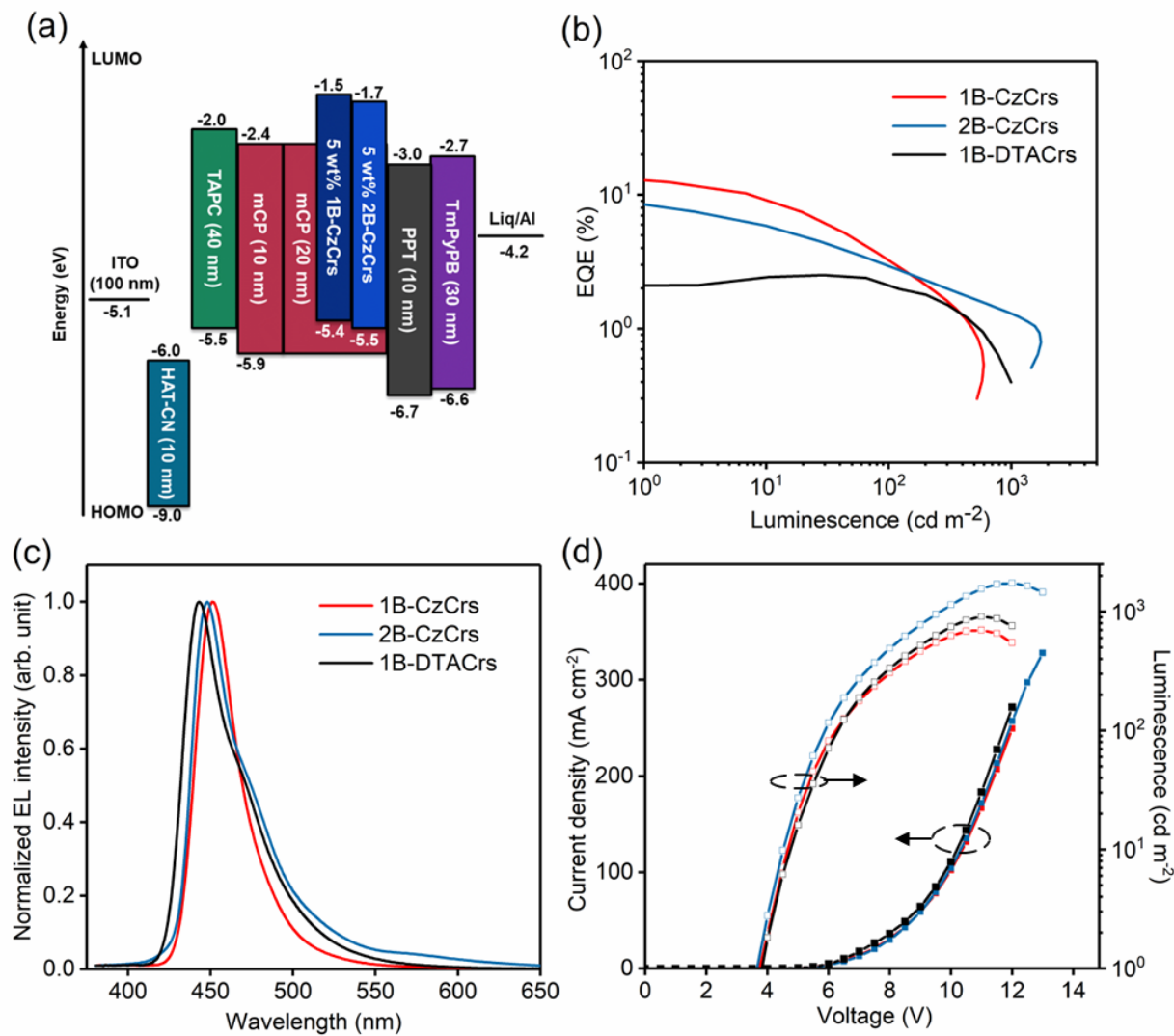Figure **S31**. Chemical structures of the compounds used for OLEDs.

Figure **S32**. Performance of devices with **1B-CzCrs** (red line), **2B-CzCrs** (blue line) and **1B-DTACrs** (black line) in **mCBP.** (a) Device structure, (b) EQE-Luminescence plot (b) EL spectra, and (d) *J-V-L* properties; current density (closed square) and luminance (open square).

Table **S10**. Device performance with an EML consisting of 5 wt% **1B-CzCrs** and **2B-CzCrs** in **mCP**.

	V_{on}^{a} (V)	EQE_{max} (%)	$EQE_{10/100/1000}$ (%)	λ_{EL} (nm)	FWHM (nm)	Lum_{max} (cd m^{-2})	$CIE_{x,y}$
1B-CzCrs	3.8	12.8[b]	9.1/ 3.3/ -	451	30	688	0.146, 0.062
2B-CzCrs	3.7	8.4[b]	5.9/ 2.9/ 1.3	450	36	1712	0.153, 0.143
1B-DTACrs	3.9	2.5[c]	2.4/ 2.0/ 0.4	443	39	902	0.155, 0.079

[a] Estimated at 1 cd m^{-2}. [b] Estimated at 1 cd m^{-2}. [c] Estimated at 28 cd m^{-2}.
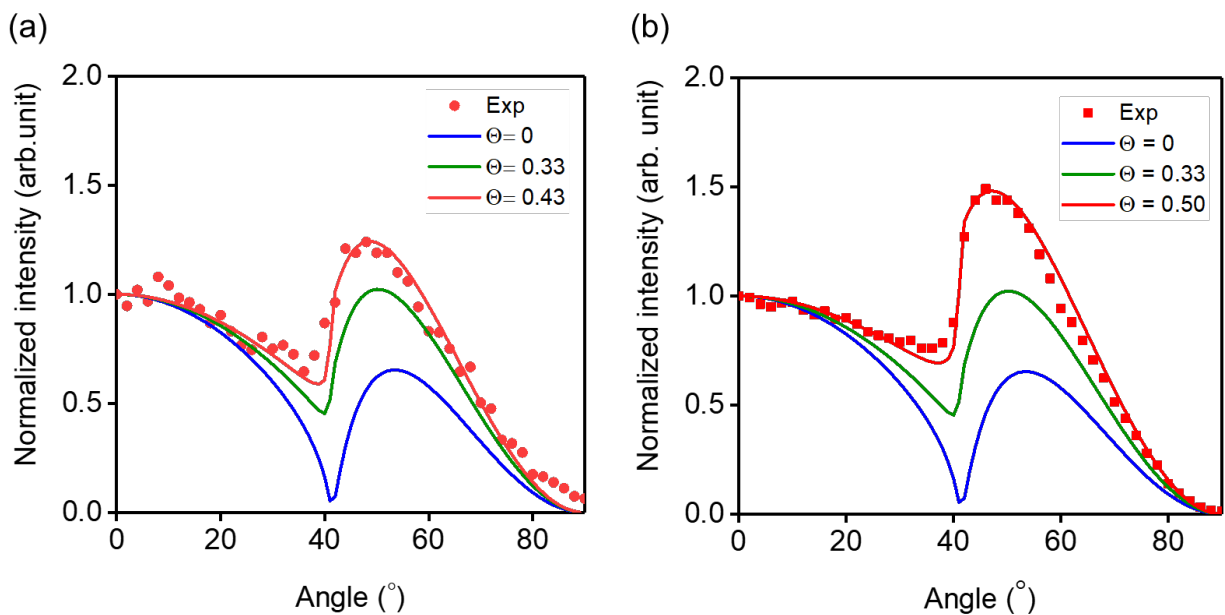
Figure S33. Angular-dependent PL profiles of 5 wt% (a) **1B-CzCrs** and (b) **2B-CzCrs** doped in **mCP**. The horizontal (blue line), isotropic (green line), and fitting curves (red line) for the experimental data (scattered plot) were provided using the optical simulation software SETFOS 5.1 (Fluxim).

Table S11. Estimated η_{oc}, theoretical EQE, and the experimental EQE for the device with **mCP** host.

	η_{oc} [b] (%)	EQE$_{\text{Theoratical}}$ [b] (%)	EQE$_{\text{Experimental}}$ (%)
1B-CzCrs	17.7	13.3	12.8
2B-CzCrs	15.3	9.5	8.4

[a] Estimated with optical simulation software SETFOS 5.1 (Fluxim), [b] Calculated with $EQE = \eta_{CB}\eta_{\gamma}\Phi_{PL}\eta_{OC}$, where η_{CB} is the charge balance factor and η_{γ} is the efficiency of radiative exciton production.[10], assuming $\eta_{CB} = \eta_{\gamma} = 1$.

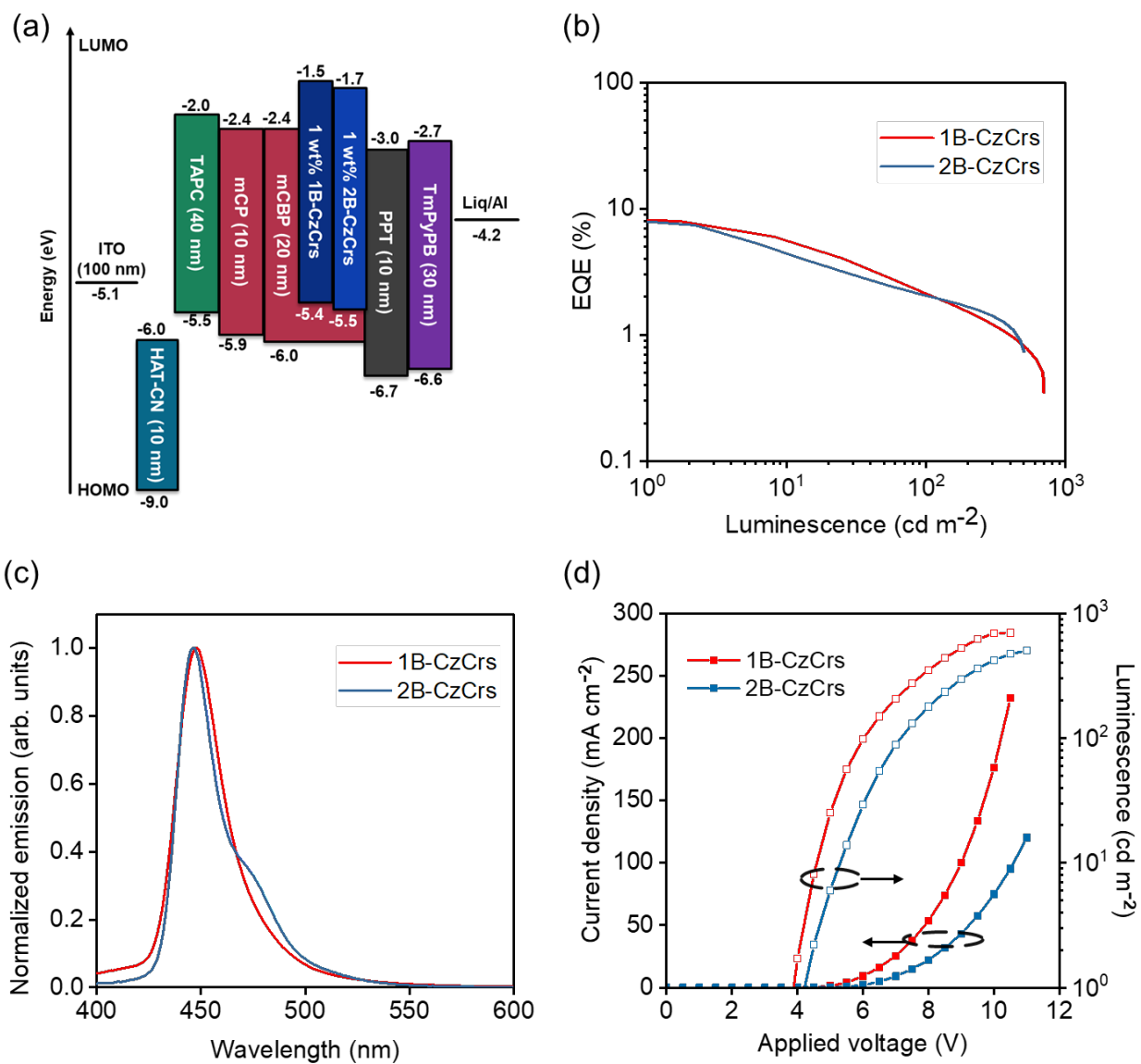Figure **S34**. Performance of devices with **1B-CzCrs** and **2B-CzCrs** in **mCBP.** (a) Device structure, (b) EQE-Luminescence plot, (c) EL spectra, and (d) *J-V-L* properties; current density (closed square) and luminance (open square).

Table **12**. Device performance with an EML consisting of 1 wt% **1B-CzCrs** and **2B-CzCrs** in **mCBP**.

Emitter	V_{on}[a] (V)	EQE_{max}[b] (%)	$EQE_{10/100}$ (%)	λ_{EL} (nm)	FWHM (nm)	Lum_{max} (cd m^{-2})	CIE_x	CIE_y
1B-CzCrs	3.9	8.1	5.6/ 2.2	448	26	705	0.152	0.048
2B-CzCrs	4.2	7.7	4.3/ 2.0	447	22	485	0.150	0.049

[a] Estimated as 1 cd m^{-2}. [b] Estimated at 1 cd m^{-2}.

References

1   G. W. T. M. J. Frisch, H. B. Schlegel, G. E. Scuseria, M. A. Robb, J. R. Cheeseman, G. Scalmani, V. Barone, G. A. Petersson, H. Nakatsuji, M. C. X. Li, A. Marenich, J. Bloino, B. G. Janesko, R. Gomperts, B. Mennucc, H. P. Hratchian, J. V. Ortiz, A. F. Izmaylov, J. L. Sonnenberg, D. Williams-Young, F. Ding, F. Lipparini, F. Egidi, J. Goings, B. Peng, A. Petrone, T. Henderson, D. Ranasinghe, V. G. Zakrzewski, J. Gao, N. Rega, G. Zheng, W. Liang, M. Hada, M. Ehara, K. Toyota, R. Fukuda, J. Hasegawa, M. Ishida, T. Nakajima, Y. Honda, O. Kitao, H. Nakai, T. Vreven, K. Throssell, J. A. Montgomery Jr., J. E. Peralta, F. Ogliaro, M. Bearpark, J. J. Heyd, E. Brothers, K. N. Kudin, V. N. Staroverov, T. Keith, R. Kobayashi, J. Normand, K. Raghavachari, A. Rendell, J. C. Burant, S. S. Iyengar, J. Tomasi, M. Cossi, J. M. Millam, M. Klene, C. Adamo, R. Cammi, J. W. Ochterski, R. L. Martin, K. Morokuma, O. Farkas, J. B. Foresman and D. J. Fox, *Gaussian 16 Rev. A.01, Inc*, Wallingford CT, 2016.

2   N. O. C. Winter and C. Hättig, *J. Chem. Phys.*, 2011, **134**, 184101.

3   TURBOMOLE V7.4 2019, a development of University of Karlsruhe and Forschungszentrum Karlsruhe GmbH, 1989-2007, TURBOMOLE GmbH, since 2007.

4   S. Hirata and M. Head-Gordon, *Chem. Phys. Lett.*, 1999, **314**, 291–299.

5   T. H. Dunning, *J. Chem. Phys.*, 1989, **90**, 1007–1023.

6   S. Grimme, *Chem. Phys. Lett.*, 1996, **259**, 128–137.

7   X. Gao, S. Bai, D. Fazzi, T. Niehaus, M. Barbatti and W. Thiel, *J. Chem. Theory Comput.*, 2017, **13**, 515–524.

8   Nielsen, A.B. and Holder, A.J. (2009) Gauss View 5.0, User's Reference. GAUSSIAN Inc.

9   K. Momma and F. Izumi, *J. Appl. Crystallogr.*, 2008, **41**, 653–658.

10   S. Lee and E. Zyzman-Colman, Silico (version **4**), DigichemCo, St Andrews, Scotland, 2023.

11   N. M. O'boyle, A. L. Tenderholt and K. M. Langner, *J. Comput. Chem.*, 2008, **29**, 839–845.

12   W. Humphrey, A. Dalke and K. Schulten, *J. Mol. Graph.*, 1996, **14**, 33–38.

13   J. Stone, Computer Science Department, University of Missouri-Rolla, 1998.

14   J. D. Hunter, *Comput. Sci. Eng.*, 2007, **9**, 90–95.

15   N. M. O'Boyle, M. Banck, C. A. James, C. Morley, T. Vandermeersch and G. R. Hutchison, *J. Cheminform.*, 2011, **3**, 33.

16   N. M. O'Boyle, C. Morley and G. R. Hutchison, *Chem. Cent. J.*, 2008, **2**, 5.

17   A. Hellweg, S. A. Grün and C. Hättig, *Phy. Chem. Chem. Phys.*, 2008, **10**, 4119.

18   F. Neese, *WIREs Comput. Mol. Sci.*, 2012, **2**, 73–78.

19   N. G. Connelly and W. E. Geiger, *Chem. Rev.*, 1996, **96**, 877–910.

20   C. M. Cardona, W. Li, A. E. Kaifer, D. Stockdale and G. C. Bazan, *Adv. Mater.s*, 2011, **23**, 2367–2371.

21   C.-Y. Chan, S. Madayanad Suresh, Y.-T. Lee, Y. Tsuchiya, T. Matulaitis, D. Hall, A. M. Z. Slawin, S. Warriner, D. Beljonne, Y. Olivier, C. Adachi and E. Zysman-Colman, *Chem.Commun.*, 2022, **58**, 9377–9380.